JOAPE

Journal of Operation and Automation in Power Engineering

Vol. XX, No. XX, XXXX, Pages: XXXX (Proofed)

http://joape.uma.ac.ir

1978 University of Mohaghegh Ardabili

Research Paper

Reliability-Driven Expert Automation Planning and Blackout Scheduling in Iranian Electricity Distribution Networks

Peyman Zare , *Hossein Shayeghi* * , and *Babak Mohamadi*

Energy Management Research Center, University of Mohaghegh Ardabili, P.O. Box 179, Ardabil, Iran.

Abstract— *Medium-voltage electricity distribution networks in Iran require automation plans that reduce customer interruptions while remaining economically defensible under harsh operating conditions. Existing planning practices often treat reliability indices as secondary outputs and rely on deterministic assumptions, which weakens device-placement decisions in long radial feeders and mountainous areas. This paper develops a reliability-driven expert automation framework for the coordinated placement of reclosers and sectionalizers, where expert automation denotes the use of utility operating rules, protection-engineering judgement, and field-experience-based uncertainty ranges, and blackout scheduling denotes feeder-level outage confinement and restoration after fault isolation. Reliability indices, undelivered energy, and equipment costs were integrated into a single objective function. Uncertainty in fault rate, outage duration, and switching time was represented by triangular fuzzy numbers and converted through defuzzification. The resulting nonlinear discrete problem was solved using Boxelder Bug Search Optimization and benchmarked against three population-based metaheuristics on a real feeder in Ardabil Province and the IEEE 33-bus system. In the real feeder, the proposed method reduced interruption frequency by up to 15.5%, interruption duration by more than 9%, and momentary interruptions by 33.0%, while lowering the composite objective value by up to 15.9%. In the benchmark system, it achieved the lowest undelivered-energy cost and objective value across all scenarios, with momentary-interruption reductions exceeding 36% under high automation. The results indicate that reliability-centred, uncertainty-aware automation planning can improve feeder-level interruption management without excessive device installation.*

Keywords—Iran electricity distribution networks, electricity distribution automation, sectionalizer and recloser placement, boxelder bug search optimization, reliability indicators.

NOMENCLATURE

Abbreviations

APED Co.	Ardabil Province Electricity Distribution Company
BBSO	Boxelder Bug Search Optimization
CVSO	Corona Virus Search Optimizer
EDA	Electricity Distribution Automation
EDN	Electricity Distribution Network
IEEE	Institute of Electrical and Electronics Engineers
MAIFI	Momentary Average Interruption Frequency Index
MTBO	Mountaineering Team-Based Optimization
SAIDI	System Average Interruption Duration Index
SAIFI	System Average Interruption Frequency Index
TFWO	Turbulent Flow of Water-Based Optimization
UE	Undelivered Energy

1. INTRODUCTION

1.1. Background and related works

Electricity distribution networks in Iran constitute a critical layer of the national power system and are subject to regulatory oversight by the Ministry of Energy, with coordination by Iran's Power Generation and Distribution Company (TAVANIR) and execution by regional and provincial distribution companies. In recent decades, rapid demand growth and network expansion have taken place across diverse geographic and climatic zones, creating persistent operational and reliability pressures. These challenges are particularly evident in the northwest of Iran, where long radial feeders, mountainous terrain, dispersed rural loads, and severe winter conditions define network operation [1].

Distribution companies in this region, including those serving Ardabil and neighboring provinces, face frequent weather-induced faults, limited physical access during outages, and extended restoration times. As a result, reliability indicators such as interruption frequency, interruption duration, and undelivered energy remain central concerns for both utilities and regulators. Electricity distribution automation has been promoted nationally as a means to improve fault isolation, accelerate service restoration, and enhance overall network resilience. Nonetheless, implementation at the distribution level is constrained by budget limitations, heterogeneous feeder characteristics, and uncertainty in fault behavior and operational response [2].

The planning and deployment of automation and protective devices in Iranian distribution networks therefore involve complex trade-offs between reliability improvement, economic feasibility, and practical operability. These constraints are amplified in the northwest region, where climatic severity and network topology intensify operational risk and planning complexity [3].

A considerable body of research has examined reliability improvement and automation planning in electricity distribution networks through optimisation, resilience analysis, and operational recovery strategies. Despite substantial progress, the manner in

Received: 27 Feb. 2026
Revised: 07 Jul. 2026
Accepted: 31 Jul. 2026
*Corresponding author:
E-mail: hshayeghi@gmail.com (H. Shayeghi)
DOI: 10.22098/joape.2026.19495.2515

which reliability indices, economic objectives, and operational uncertainty are jointly incorporated into automation planning remains limited. Most existing studies address these aspects separately, which restricts their applicability to practical feeder-level planning in distribution systems operating under variable climatic conditions. A major stream of research has focused on the optimal allocation of switching and protective devices as a planning problem. Researchers [4] proposed a multi-objective cross-entropy approach for recloser placement, demonstrating the ability to generate Pareto-efficient solutions based on interruption and cost criteria. Similarly, authors [5] investigated switch allocation using evolutionary algorithms, allowing both manual and remotely controlled switches to be optimised without predefined limits. Although these studies advanced algorithmic optimisation, they primarily emphasised solution quality and convergence behaviour, while cross-scenario operational uncertainty was not explicitly represented. In a different direction, in Ref. [6] A mixed-integer linear model was formulated for the coordination of protective and switching devices in active distribution networks, providing a rigorous optimisation structure but relying on deterministic parameter assumptions. The work reported in Ref. [7] further extended device installation planning through a multi-objective formulation incorporating interruption costs and voltage constraints, yet uncertainty in fault and restoration parameters was not explicitly modelled. Collectively, these works demonstrate the feasibility of optimisation-based device allocation, while revealing a persistent gap in integrating reliability indices and uncertainty within a unified planning framework.

Another group of studies has concentrated on resilience-oriented planning under extreme events. Researchers [8] developed a planning model that jointly considered distribution automation and energy storage investments to enhance resilience against hurricanes. Authors [9] proposed a resilience-focused framework for deploying remote-controlled switches and soft open points under thunderstorm disasters, while in Ref. [10] reliability-oriented planning of hybrid AC/DC distribution networks incorporating risk assessment was examined. These studies highlight the importance of automation under high-impact disruptions; however, their formulations are largely event-specific and do not directly address coordinated sectionalizer and recloser placement driven by routine reliability indices under general operating uncertainty.

Several works have addressed reliability and resilience assessment rather than automation investment decisions. Researchers [11] employed data envelopment analysis to determine economically efficient reliability targets for distribution systems, focusing on benchmarking rather than device placement. In Ref. [12], smart switch placement was linked to reliability indices via topology-dependent decision variables in flexible distribution networks, which may not account for conventional feeder automation constraints. The study in Ref. [13] presented an analytical method for assessing reliability and resilience in systems with mobile power sources, while the authors in Ref. [14] quantified the impact of overhead-to-underground cable ratios on reliability indices. Although these studies improve understanding and measurement of reliability performance, they stop short of solving coordinated automation planning problems with explicit investment decisions.

A further body of literature has examined post-fault operation and emergency response. Researchers [14] formulated an optimisation model for emergency load shedding under stability constraints, and the authors [15] developed a restoration strategy incorporating differentiated customer reliability demands. In Ref. [16], distribution network gray-start and emergency recovery considering remote-controlled switches were investigated, while the framework in Ref. [17] proposed a flexible scheduling strategy to reduce outage impacts. These contributions address critical operational stages following disturbances, yet they treat automation infrastructure as given and do not integrate long-term placement decisions with reliability-driven planning objectives.

Finally, some studies have focused on blackout propagation and protection performance at a broader system level. Researchers [18] evaluated protection solutions for embedded microgrids, and the authors [19] investigated reliability improvement through microgrids and auxiliary services.

Taken together, the reviewed studies indicate that, despite advances in optimisation, resilience analysis, and reliability assessment, a clear gap remains in developing an integrated automation planning framework that treats reliability indices as primary decision variables, incorporates economic considerations, and explicitly accounts for operational uncertainty. This gap is particularly evident for medium-voltage distribution feeders operating under diverse climatic conditions, motivating the reliability-driven and uncertainty-aware planning approach proposed in this study.

To clarify the positioning of the present study with respect to recent research and to highlight its distinguishing methodological features, a taxonomy-based comparison is constructed in Table 1.

1.2. Main contributions

This study addresses three limitations that remain only partly resolved in recent work on distribution automation planning. First, many studies assess reliability improvement after device placement, while the reliability indices themselves are not embedded in the optimization objective. This treatment weakens the link between the planning decision and the reliability targets expected by distribution utilities. Second, uncertainty in fault rate, repair duration, and switching time is often represented through deterministic values or simplified sensitivity cases, although these variables are strongly affected by seasonal weather, feeder accessibility, and field-operation constraints. Third, the comparison of metaheuristic solvers is commonly restricted to final objective values, with limited discussion of search behaviour, computational consistency, and performance across both practical and benchmark networks.

To address these gaps, this paper develops a reliability-driven expert automation planning framework for the coordinated placement of reclosers and sectionalizers in medium-voltage distribution networks. The proposed framework integrates SAIFI, SAIDI, MAIFI, undelivered energy, and device investment cost into a unified objective function, so reliability is treated as a core planning target rather than as a post-processing index. Operational uncertainty is represented by triangular fuzzy numbers for fault rate, outage duration, and switching time, with fuzzy bounds derived from historical records and utility operating experience. In this sense, the expert component of the framework is reflected in the use of protection-engineering practice, feasible device-location rules, and field-experience-based uncertainty ranges. The advantage of the proposed method is that it links automation investment directly to measurable reliability and interruption-cost outcomes under climate-dependent operating conditions. The framework also supports blackout-oriented scheduling at the feeder level by reducing the frequency, duration, and extent of supply interruptions through coordinated placement of protective devices. The resulting nonlinear and discrete optimization problem is solved using BBSO and compared with MTBO, CVSO, and TFWO under the same computational protocol. Validation is performed on a real feeder in Ardabil Province and the IEEE 33-bus benchmark system, allowing the performance of the method to be examined under both utility-scale and standard test-network conditions. Fig. 1 summarizes the main workflow of the proposed planning framework.

The main contributions of this research are outlined as follows:

(1) Reliability-centred optimization formulation: This research introduces a unified objective function that integrates multiple reliability indices with economic cost terms, rather than treating reliability as a post-optimization evaluation metric.

(2) Fuzzy-based representation of operational uncertainty: This study establishes a structured fuzzy modeling approach to represent uncertainty in fault occurrence, restoration duration, and

Table 1. Taxonomy of recent distribution automation planning studies.

Ref.	Reliability indices objective	Sectionalizer recloser Placement	Uncertainty modeling layer	Population-based metaheuristic optimization	Multi-scenario climate/Extreme-event analysis	Joint cost reliability trade-off	Real-feeder utility validation	Blackout/Emergency scheduling focus
[13]	×	×	×	×	✓	✓	×	×
[11]	✓	×	×	✓	×	✓	×	×
[10]	✓	✓	×	✓	×	✓	×	✓
[9]	✓	✓	×	✓	×	✓	×	✓
[8]	✓	✓	✓	✓	✓	✓	×	✓
[7]	✓	×	×	✓	✓	✓	✓	✓
[6]	✓	×	✓	✓	×	✓	✓	×
[5]	✓	×	✓	✓	✓	✓	✓	×
[4]	✓	×	✓	✓	×	✓	✓	×
[12]	✓	✓	✓	✓	×	✓	✓	✓
[3]	✓	✓	✓	✓	×	×	✓	✓
[2]	×	✓	✓	✓	×	×	×	✓
[1]	✓	✓	×	×	×	✓	✓	✓
Present work	✓	✓	✓	✓	✓	✓	✓	✓

operations, reflecting real operational conditions in climatically harsh regions.

(3) Metaheuristic optimization for discrete automation planning: This work applies and validates the BBSO algorithm, and competing algorithms such as MTBO, CVSO, TFWO for the coordinated placement of sectionalizers and reclosers in medium-voltage distribution networks.

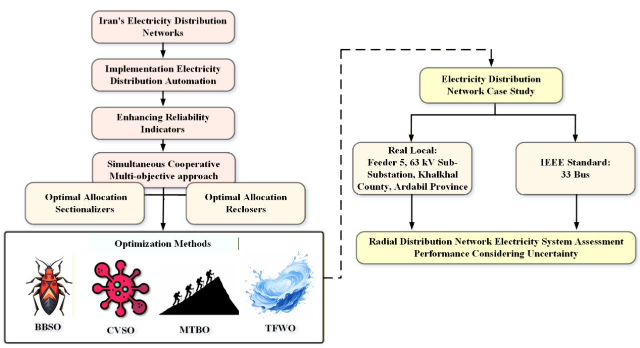

Fig. 1. Overall workflow of the proposed reliability-driven automation planning framework.

The remainder of this paper is organized as follows. Section 2 presents the conceptual and operational framework for electricity distribution automation. Section 3 formulates the proposed optimization problem, while Section 4 discusses the numerical results and comparative analysis. Finally, Section 5 concludes the paper.

2. Conceptual and Operational Framework for Electricity Distribution Automation

2.1. Concept of expert electricity distribution automation for blackout scheduling

Electricity distribution automation refers to the use of remotely or automatically operated protection and switching devices to detect faults, isolate affected feeder sections, and restore healthy load areas with minimal delay. In radial medium-voltage networks, this process depends strongly on the number and location of reclosers and sectionalizers. A recloser can clear transient faults and restore supply automatically, whereas a sectionalizer divides the feeder into smaller protection zones and prevents permanent faults from affecting a larger customer area.

In the present study, expert automation is defined as an automation planning process that combines mathematical optimization with practical knowledge from distribution-system operation. This knowledge includes admissible device locations, feeder accessibility, protection coordination rules, typical switching times, fault exposure of overhead sections, and utility experience under cold and mountainous conditions. These elements are introduced into the model through candidate-location constraints, fuzzy uncertainty ranges, and reliability-oriented objective terms. The proposed planning framework therefore reflects the way automation decisions are made in real distribution companies, where engineering judgement and historical field data complement numerical optimization.

Blackout scheduling is treated as a feeder-level reliability-management concept. It does not refer to system-wide cascading blackout analysis. Instead, it represents the planned organization of interruption confinement and service restoration after a distribution fault. When a fault occurs, the installed reclosers and sectionalizers determine which feeder segments are disconnected, which load points remain energized, and how rapidly the healthy sections can be restored. The scheduling effect is therefore captured through outage duration, switching time, customer interruption indices, and undelivered energy. Under this interpretation, the optimization model schedules blackout mitigation indirectly by selecting device locations that minimize the size, frequency, and duration of feeder-level supply interruptions.

2.2. Geographic characteristics of Ardabil province

Ardabil Province is located in northwestern Iran and forms part of the national border zone with the Republic of Azerbaijan to the north. Territorial adjacency extends toward East Azerbaijan, Zanjan, and Gilan along its western and southern margins. The administrative centre is the city of Ardabil. Provincial status was assigned in 1993 following separation from East Azerbaijan.

Climatic conditions are severe during winter months. Air temperatures can decline to minus twenty-five degrees Celsius, placing the province among the coldest areas in the country. This thermal profile is closely associated with the Sabalan mountain range, whose elevation and geomorphology influence local atmospheric conditions. Forested areas cover a substantial share of the territory and contribute to regional environmental characteristics.

The provincial capital lies at an approximate distance of seventy kilometres from the Caspian Sea and the province encompasses a land area of eighteen thousand and eleven square kilometres. Geographic proximity to the Caspian basin and direct access to an international boundary confer political and economic relevance at both regional and national levels. From an administrative perspective, the province is organised into twelve counties: Ardabil, Bila Savar, Germi, Khalkhal, Kowsar, Meshginshahr, Namin, Sarein, Nir, Ungut, Aslan Duz, and Parsabad [20].

2.3. Overview of the Ardabil province electricity distribution company

The APED Co. is responsible for electricity distribution across Ardabil Province within Iran's power system. Its activities cover network operation and expansion, maintenance, load control, and customer services, supplying electricity to residential, commercial, industrial, agricultural, and public users.

Electricity services in Ardabil began in the 1930s and were later administered by regional authorities until the province gained independent status in 1993. Following this transition, APED Co. was established under the Ministry of Energy to manage provincial distribution networks. Since then, the company has developed a wide-ranging infrastructure that includes high-, medium-, and low-voltage networks, multiple substations, and a large population of distribution transformers. By the early 2026s, this system supported electricity delivery across all counties of the province through a decentralised organisational structure [20].

2.4. Khalkhal city case description

The deployment of an EDA system within the Ardabil Province Electricity Distribution Company requires substantial organisational effort and extended implementation time. This stems from the need to establish an underlying platform capable of supporting EDA design and operation. For this reason, a detailed needs assessment and feasibility analysis must be conducted in advance, with attention given to technical constraints and system requirements.

Khalkhal County is located in the southern part of Ardabil Province, Iran, with the city of Khalkhal serving as its administrative centre. The area is predominantly mountainous and experiences a cold climate, particularly in and around the urban core. In demographic terms, Khalkhal is the fourth most populated city in the province. The county spans approximately three thousand nine hundred and eighty square kilometres and accommodates a population of eighty six thousand seven hundred and thirty one residents. Administratively, it includes three cities, Khalkhal, Hashjin, and Kalor, and three districts: Markazi, Khoresh Rostam, and Shahroud.

Electricity distribution within the county is managed by the Khalkhal Electricity Management Department, which operates under the supervision of the Ardabil Province Electricity Distribution Company. Power supply to Khalkhal is delivered through six feeder lines originating from a 63 kV sub-distribution substation. Feeder 1 extends toward Kivi and supplies several internal feeders within Khalkhal City. Feeder 4 provides the connection between Khalkhal and Hashjin, while Feeder 5 serves areas leading toward the Shahroud districts.

Feeder 5 originates at the 63 kV sub-distribution substation in Khalkhal City and extends toward the Shahroud districts. It is the second longest feeder in the county, surpassed only by Feeder 4. The total length reaches one hundred and eighty kilometres, comprising a thirty six kilometre main section and one hundred and forty four kilometres of secondary lines. Along this route, one hundred and fifty seven overhead distribution transformers are installed. The feeder traverses mountainous terrain and remote areas, which increases exposure to operational stress and places it among the more vulnerable components of the provincial electricity distribution network. Electricity is supplied to multiple villages branching toward Shahroud through this feeder. Its peak load reaches one hundred and twenty amperes, and the conductors used have cross-sectional areas of thirty five, seventy, and one hundred and twenty six square millimetres.

3. Problem Formulation

This section presents the mathematical formulation developed to support the optimal deployment of EDA devices in medium-voltage EDNs. The formulation targets the coordinated placement of protective equipment, with emphasis on sectionalizers and reclosers, in order to improve service reliability while controlling total system cost. The problem is posed as a constrained multi-criteria optimization task, where technical performance and economic efficiency are treated jointly.

The planning objective reflects the operational reality of Iranian EDNs. Reliability improvement cannot be pursued independently of investment limitations, nor can cost minimization be addressed without explicit consideration of customer interruptions and undelivered energy.

3.1. Objective function

The objective function is defined as a weighted aggregation of economic cost terms and system reliability indices. The goal is to minimize the composite objective value through optimal selection and placement of EDA devices across candidate locations in the network:

$$\begin{aligned} \min\ OF = w_1 E_{\mathrm{UE}} + w_2\left(E_{\mathrm{UE}} \cdot \mathrm{SAIDI}\right) + \\ w_3 \mathrm{SAIFI} + w_4 \mathrm{MAIFI} + w_5 C_{\mathrm{eq}} \end{aligned} \tag{1}$$

where E_{UE} denotes the expected undelivered energy, SAIDI, SAIFI, and MAIFI represent standard reliability indices, and C_{eq} corresponds to the total investment cost associated with protective equipment. The coefficients w_i are weighting factors that regulate the relative influence of each term and satisfy the normalization condition.

$$\sum_{i=1}^{5} w_i = 1 \tag{2}$$

The weighting coefficients in the objective function were determined using a normalized priority-based procedure. Since the objective function combines reliability indices, undelivered energy, and equipment investment cost, all objective components were first converted into dimensionless terms using reference values. The reference values of SAIFI, SAIDI, MAIFI, and EUE were obtained from the base feeder without additional automation, while the equipment-cost reference was defined according to the maximum allowable investment level considered in the planning problem. This normalization prevents the objective function from being dominated by the numerical scale or physical unit of any single term.

The baseline weight vector was then assigned according to utility planning priorities in harsh climatic regions. Sustained interruption duration and undelivered energy were given the highest priority because they directly reflect restoration difficulty, customer supply interruption, and energy-not-supplied cost. Interruption frequency was assigned the next priority, while momentary interruptions and equipment cost were retained with lower but non-negligible weights to preserve the balance between reliability improvement and investment limitation. Accordingly, the baseline coefficients were defined as $w_{EUE} = 0.25$, $w_{SAIDI} = 0.25$, $w_{SAIFI} = 0.20$, $w_{MAIFI} = 0.15$, and $w_{Ceq} = 0.15$.

This structure allows planners to balance economic and technical priorities in line with operational policies or regulatory requirements. Reliability indices are explicitly embedded rather than treated as secondary constraints, enabling direct trade-offs between interruption performance and expenditure.

The undelivered energy term is expressed as:

$$E_{\mathrm{UE}} = \sum_{l \in \mathcal{L}} \lambda_l T_l P_l \tag{3}$$

where λ_l is the fault rate of line l, t_l is the average outage duration associated with that line after protective action, and P_l denotes the connected load. The values of t_l depend on the type, number, and location of installed sectionalizers and reclosers, thereby linking equipment placement directly to energy not supplied.

Reliability indices are computed according to standard definitions:

$$\mathrm{SAIFI} = \frac{\sum_{k\in\mathcal{K}} N_k \lambda_k}{\sum_{k\in\mathcal{K}} N_k} \tag{4}$$

$$\lambda = \frac{MMG\ losses\ considering\ with\ DG}{MMG\ losses\ without\ DG} \tag{5}$$

$$\mathrm{MAIFI} = \frac{\sum_{k\in\mathcal{K}} N_k \lambda_k^{\mathrm{tr}}}{\sum_{k\in\mathcal{K}} N_k} \tag{6}$$

where N_k represents the number of customers at load point k, T_k is the average interruption duration, and λ_k^{tr} denotes the transient fault rate contributing to momentary interruptions.

The blackout-scheduling aspect is embedded in the optimization model through the dependence of outage duration, switching time, and undelivered energy on the installed protection devices. Each candidate placement defines a different post-fault isolation and restoration sequence: upstream reclosers accelerate transient fault clearing, while downstream sectionalizers restrict permanent-fault interruptions to smaller feeder zones. The resulting interruption pattern is reflected in SAIFI, SAIDI, MAIFI, and EUE, which allows the model to evaluate blackout confinement and restoration scheduling within the same objective function.

3.2. Cost modeling

The total equipment cost is formulated as:

$$C_{\mathrm{eq}} = n_{\mathrm{rec}} C_{\mathrm{rec}} + n_{\mathrm{sec}} C_{\mathrm{sec}} \tag{7}$$

where n_{rec} and n_{sec} are the numbers of installed reclosers and sectionalizers, and C_{rec}, C_{sec} denote their respective unit costs. This formulation assumes fixed procurement and installation costs, consistent with planning-stage analysis.

3.3. Constraints

The optimization problem is subject to several technical and economic constraints that ensure feasibility and operational acceptability.

A) Budget constraint

$$C_{\mathrm{eq}} \le C_{\mathrm{MAX}} \tag{8}$$

where C_{MAX} defines the maximum allowable investment budget.

B) Reliability bounds

$$\mathrm{SAIFI}_{\min} \le \mathrm{SAIFI} \le \mathrm{SAIFI}_{\max} \tag{9}$$

$$\mathrm{SAIDI}_{\min} \le \mathrm{SAIDI} \le \mathrm{SAIDI}_{\max} \tag{10}$$

$$\mathrm{MAIFI}_{\min} \le \mathrm{MAIFI} \le \mathrm{MAIFI}_{\max} \tag{11}$$

These bounds reflect acceptable service quality levels imposed by regulatory standards or utility policies.

C) Placement constraints

$$x_i \in \{0,1\}, \quad \forall i \in \mathcal{N} \tag{12}$$

where x_i indicates whether a protective device is installed at candidate location i. Only one device type may be assigned to a given location, and installation is restricted to predefined feasible nodes.

D) Network topology constraints

Power flow continuity and the radial operating structure of the distribution network are maintained following the installation of protective devices. Switching and protection actions are constrained such that feeder connectivity is preserved and no load points become electrically isolated under normal operating conditions. The detailed network constraints governing topology, connectivity, and operational feasibility are adopted from [15] and are therefore not restated here.

3.4. Uncertainty representation

Uncertainty is an inherent characteristic of EDNs, particularly with respect to fault occurrence, restoration duration, and operator response. In practical operation, these parameters are influenced by weather conditions, terrain, protection coordination, and human decision-making. Treating such variables as deterministic quantities may distort reliability assessment and lead to suboptimal placement of EDA devices. To address this issue, uncertainty is represented through fuzzy modeling of selected parameters.

In this study, fault rates, outage durations, and switching times are modeled as fuzzy variables. Each uncertain parameter is described using a triangular fuzzy number, which captures minimum, most likely, and maximum values derived from historical data and operational experience. Triangular fuzzy numbers were selected because the uncertainty considered in this study is mainly planning-level and operational, rather than a high-resolution stochastic process with a known probability distribution. In the studied feeders, fault rate, outage duration, and switching time are influenced by weather severity, feeder accessibility, protection coordination, crew response, and local field conditions. These factors are not always supported by sufficiently long and homogeneous statistical records, especially under severe winter conditions. A triangular representation is therefore suitable because it requires only three interpretable values: a lower bound, a most probable value, and an upper bound. These values can be obtained from historical utility records, maintenance reports, and operator experience, while avoiding unsupported assumptions about normal, Weibull, or other parametric distributions. The method is also computationally compatible with the proposed metaheuristic optimization, since the centroid defuzzification step provides a stable crisp equivalent at each fitness evaluation without increasing the computational burden.

For a generic uncertain parameter $\tilde{x}$, the fuzzy representation is defined as:

$$\tilde{x} = \left(x^{\min}, x^{\mathrm{nom}}, x^{\max}\right) \tag{13}$$

where x^{min} and x^{max} denote the lower and upper bounds of uncertainty, and x^{nom} represents the most probable value.

Accordingly, the fault rate of line l, outage duration at load point k, and switching time associated with protective device iare expressed as:

$$\tilde{\lambda}_l = \left(\lambda_l^{\min}, \lambda_l^{\mathrm{nom}}, \lambda_l^{\max}\right) \tag{14}$$

$$\tilde{T}_k = \left(T_k^{\min}, T_k^{\mathrm{nom}}, T_k^{\max}\right) \tag{15}$$

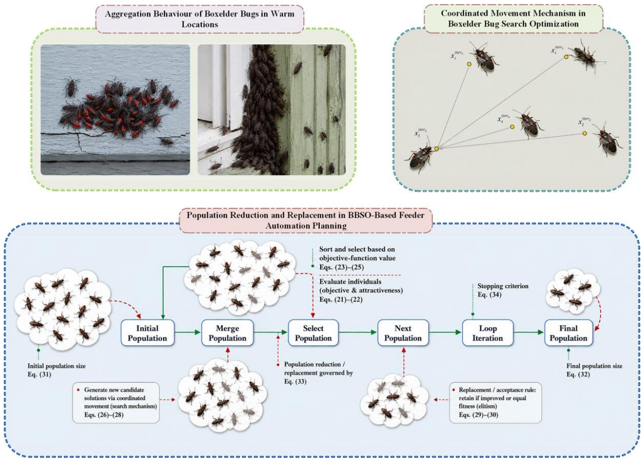

Fig. 2. Conceptual framework of Boxelder Bug search optimization for recloser and sectionalizer placement in distribution feeder automation.

$$\tilde{t}_i = \left(t_i^{\min}, t_i^{\text{nom}}, t_i^{\max}\right) \tag{16}$$

These fuzzy variables are propagated through the reliability and energy not supplied calculations. As a result, undelivered energy and reliability indices become fuzzy quantities. For example, the fuzzy expected undelivered energy is obtained as:

$$\tilde{E}_{\text{UE}} = \sum_{l \in \mathcal{L}} \tilde{\lambda}_l \tilde{T}_l P_l \tag{17}$$

Similarly, fuzzy forms of the reliability indices are computed by replacing deterministic parameters in Eqs. (4)-(6) with their fuzzy counterparts.

To enable compatibility with the optimization algorithm, defuzzification is applied during the fitness evaluation stage. The centroid method is adopted to convert each fuzzy variable into a crisp equivalent. For a generic fuzzy parameter $\tilde{x}$, the defuzzified value x^* is obtained as:

$$x^* = \frac{x^{\min} + x^{\text{nom}} + x^{\max}}{3} \tag{18}$$

Defuzzified values are then used to evaluate the objective function and constraints at each iteration of the optimization process. The fuzzy uncertainty layer and the weighting structure have different roles in the proposed formulation. The fuzzy layer represents operational uncertainty in fault rate, outage duration, and switching time. These parameters are affected by climatic severity, feeder accessibility, protection response, and field-operation conditions. Each uncertain parameter is represented by a triangular fuzzy number, whose lower, modal, and upper bounds describe the optimistic, most likely, and pessimistic operating conditions. After defuzzification, these uncertain parameters are used to calculate the crisp equivalent values of reliability indices and undelivered energy during fitness evaluation. The weighting coefficients are not treated as fuzzy variables. They represent the planner's preference among normalized objective components after uncertainty has been processed. In other words, fuzzy modelling captures uncertainty in the physical and operational input parameters, whereas the weighting coefficients express the relative importance assigned to reliability, undelivered energy, and investment cost. The robustness of these preference coefficients is therefore examined separately through sensitivity analysis.

The expert component of the framework is introduced at this stage by defining the lower, nominal, and upper bounds of each triangular fuzzy number from both historical records and utility operating experience. For example, severe winter access limitations, mountainous feeder exposure, and typical crew response times are reflected in the fuzzy bounds assigned to outage duration and switching time.

3.5. Solution method

The formulated automation-planning problem is nonlinear, discrete, and combinatorial because the decision variables determine the placement of reclosers and sectionalizers over a finite set of candidate feeder locations. Each candidate solution must satisfy technical placement constraints, device-count limitations, and the reliability-cost trade-off defined in the objective function. Exhaustive enumeration becomes impractical when the number of candidate branches increases, since every additional candidate location enlarges the binary search space. For this reason, a population-based metaheuristic solution framework is adopted.

In this study, the Boxelder Bug Search Optimization (BBSO) algorithm is used as the main optimizer. BBSO is a bio-inspired search method derived from the seasonal migration and group behaviour of boxelder bugs (Boisea trivittata) [21]. These insects tend to move toward warmer places during cold seasons, aggregate around favourable locations, and maintain group movement while a portion of the population may be lost or replaced. In the optimization context, these behaviours are translated into three computational operators: movement toward high-quality candidate solutions, coordinated population movement, and controlled population reduction/replacement. Fig. 2 illustrates these main behavioural phases, while Algorithm 1 presents the pseudo-code used for implementing the BBSO-based automation-planning procedure.

The solution process begins by encoding each candidate automation plan as a discrete vector. For a feeder with N_c candidate locations, the i-th individual in the BBSO population is defined as:

$$\begin{aligned} &\mathbf{x}_i^{\text{Iter}} = \\ &\left[y_{i,1}^R, y_{i,2}^R, \ldots, y_{i,N_c}^R, y_{i,1}^S, y_{i,2}^S, \ldots, y_{i,N_c}^S\right]^{\text{Iter}}, \quad i = 1, 2, \ldots, n_{\text{pop}} \end{aligned} \tag{19}$$

where $y_{i,k}^R$ and $y_{i,k}^S$ are binary placement variables for a recloser and a sectionalizer at candidate location k, respectively. A value of one indicates that the corresponding device is installed, while a value of zero indicates that it is not selected. To avoid simultaneous installation of both devices at the same candidate location, the following feasibility condition is imposed:

$$y_{i,k}^R + y_{i,k}^S \leq 1, \qquad k = 1, 2, \ldots, N_c \tag{20}$$

Each individual is evaluated by the objective function developed in the previous section. Since the problem is formulated as a minimization problem, a lower objective-function value indicates a better automation plan. The fitness value of the i-th individual at iteration Iteris therefore expressed as:

$$J_i^{\text{Iter}} = OF\left(\mathbf{x}_i^{\text{Iter}}\right) \tag{21}$$

where $OF(\cdot)$ denotes the normalized objective function that includes the reliability indices, undelivered energy, and equipment investment cost. In the BBSO mechanism, a warm location corresponds to a more attractive solution. Since better solutions have lower objective-function values, the temperature associated with each candidate solution is defined as the inverse of its fitness value:

$$T_i^{\text{Iter}} = \frac{1}{J_i^{\text{Iter}} + \varepsilon} \tag{22}$$

where ε is a small positive value used to avoid division by zero. According to Eq. (22), a candidate solution with a lower objective-function value has a higher temperature and becomes more attractive for the movement of other individuals. This definition provides the mathematical basis for the first BBSO phase shown in Fig. 2, namely the search for warmer and more favourable regions of the solution space.

After fitness evaluation, the population is sorted according to the objective-function value:

$$J_{\pi(1)}^{\text{Iter}} \leq J_{\pi(2)}^{\text{Iter}} \leq \cdots \leq J_{\pi(n_{\text{pop}})}^{\text{Iter}} \tag{23}$$

where $\pi(\cdot)$ denotes the ranking index after sorting. The first individual in the sorted list corresponds to the best candidate solution in the current population. This ranking is required for the coordinated movement phase, because lower-quality individuals are guided by better-performing members while still maintaining stochastic deviations.

To normalize fitness information across the population, the average fitness value is calculated as:

$$Sfr^{\text{Iter}} = \frac{1}{n_{\text{pop}}} \sum_{t=1}^{n_{\text{pop}}} J_t^{\text{Iter}} \tag{24}$$

The relative fitness ratio of the i-th individual is then defined as:

$$fri_i^{\text{Iter}} = \frac{J_i^{\text{Iter}}}{Sfr^{\text{Iter}}} \tag{25}$$

where fri_i^{Iter} measures the relative quality of individual iwith respect to the population average. For a minimization problem, values lower than one indicate individuals that perform better than the population mean, whereas values greater than one indicate weaker candidate solutions. This ratio controls the intensity of stochastic movement and prevents the population from collapsing too early around a single candidate solution.

The coordinated movement of boxelder bugs is mathematically represented by updating each decision variable of an individual according to the position of better-ranked individuals, local directional movement, and a random perturbation term. For the j-th dimension of the i-th individual, the continuous update equation is written as:

$$\begin{aligned} x_{i,j}^{\text{New}} &= x_{\pi(i),j}^{\text{Iter}} + r_{1,j}\left(x_{\pi(i),j}^{\text{Iter}} - x_{i,j}^{\text{Iter}}\right) + \\ & r_{2,j}\left(x_{\pi(i-1),j}^{\text{Iter}} - x_{\pi(i),j}^{\text{Iter}}\right) + \frac{r_{1,j} r_{c,j}}{fri_i^{\text{Iter}} n_{\text{pop}}} x_{\pi(i),j}^{\text{Iter}} \end{aligned} \tag{26}$$

where $x_{i,j}^{New}$ is the newly generated value of the j-th decision variable, $x_{\pi(i),j}^{Iter}$ is the corresponding variable of the ranked individual, and $x_{\pi(i-1),j}^{Iter}$ represents the preceding better-ranked individual. The random coefficients $r_{1,j}$ and $r_{2,j}$ are generated in the interval [0,1], while $r_{c,j}$ is generated in the interval [-0.5,0.5]. The first movement term guides individuals toward more attractive solutions. The second term introduces coordinated swarm movement by using the relative position of better-ranked individuals. The final term introduces controlled random deviation, scaled by the relative fitness ratio and the current population size. This structure enables exploitation around promising automation plans while retaining enough diversity to explore alternative device-placement patterns.

Because Eq. (26) may generate values outside the admissible range, a boundary-control rule is applied before discrete conversion:

$$x_{i,j}^{\text{New}} = \min\left\{x_j^{\max}, \max\left(x_j^{\min}, x_{i,j}^{\text{New}}\right)\right\} \tag{27}$$

where x_j^{min} and x_j^{max} are the lower and upper limits of the j-th decision variable. Since the automation-placement problem is discrete, the updated continuous values are converted into binary placement decisions using a threshold-based mapping:

$$z_{i,j}^{\text{New}} = \begin{cases} 1, & x_{i,j}^{\text{New}} \geq \tau_j \\ 0, & x_{i,j}^{\text{New}} < \tau_j \end{cases} \tag{28}$$

where $z_{i,j}^{New}$ is the repaired binary value and τ_j is the threshold assigned to the j-th decision variable. In this study, the threshold is set to 0.5 for binary recloser and sectionalizer placement variables. After binary conversion, the repair procedure checks all technical constraints, including device exclusivity at each candidate location, maximum number of installable devices, and budget feasibility. If a solution violates these constraints, the infeasible entries are corrected by removing the least beneficial device locations based on their contribution to the objective-function value.

The updated solution is accepted only when it improves or preserves the fitness of the previous solution. The replacement rule is defined as:

$$\mathbf{x}_i^{\text{Iter}} = \begin{cases} \mathbf{x}_i^{\text{New}}, & J\left(\mathbf{x}_i^{\text{New}}\right) \leq J\left(\mathbf{x}_i^{\text{Iter}-1}\right) \\ \mathbf{x}_i^{\text{Iter}-1}, & \text{otherwise} \end{cases} \tag{29}$$

This acceptance rule prevents the algorithm from losing a previously obtained high-quality automation plan. After all individuals are evaluated, the global best solution is updated as follows:

$$z_{i,j}^{\text{New}} = \begin{cases} 1, & x_{i,j}^{\text{New}} \geq \tau_j \\ 0, & x_{i,j}^{\text{New}} < \tau_j \end{cases} \tag{30}$$

The third behavioural mechanism of BBSO is mortality and replacement. In natural migration, some boxelder bugs may leave the swarm or fail to survive unfavourable conditions. In the algorithmic form, this behaviour is used to regulate the population size and maintain search diversity during the early iterations, while gradually increasing exploitation pressure near the end of the search. The initial population size is selected as a multiple of the problem dimension:

$$n_{\text{pop}}^{\text{init}} = 5D \tag{31}$$

where D is the number of decision variables in the encoded automation-planning vector. During the search process, the population size is gradually reduced until it approaches the dimension of the problem:

$$n_{\text{pop}}^{\text{final}} \approx D \tag{32}$$

The population-reduction rule is expressed as:

$$n_{\text{pop}}^{\text{Iter}+1} = \max\left[n_{\text{pop}}^{\text{final}}, \text{ round}\left(n_{\text{pop}}^{\text{Iter}} - N_w n_{\text{pop}}^{\text{Iter}} \frac{\text{Iter}}{\text{MaxIter}}\right)\right] \tag{33}$$

where $N_w \in [0.1, 0.9]$ is the population-reduction coefficient and MaxIteris the maximum number of iterations. At each reduction stage, the old and newly generated individuals are merged, sorted according to their objective-function values, and only the best-performing individuals are retained. This strategy reduces redundant weak solutions, keeps the search focused on high-quality regions, and improves convergence robustness without suppressing early-stage exploration.

The iterative procedure continues until the predefined stopping criterion is reached:

$$\text{Iter} = \text{MaxIter} \tag{34}$$

Algorithm 1	**BBSO-based solution procedure for coordinated recloser and sectionalizer placement**
Input:	feeder topology, candidate device locations, climatic scenario data, objective weights, $n_{\rm pop} = 50$, MaxIter $= 30$, and reduction coefficient N_w.
Output:	Best automation plan $X_{\rm best}$, final reliability indices, EUE, and investment cost.
Procedure	**BBSO**
	Generate the initial population of feasible device-placement vectors using Eq. (19).
	Repair candidates that violate location exclusivity, device-count, or budget limits.
	Evaluate SAIFI, SAIDI, MAIFI, EUE, equipment cost, and the objective value for each candidate.
	Set $X_{\rm best}$ as the candidate with the minimum objective-function value.
	while Iter $<$ MaxIter **do**
	Sort the population by objective value and compute S_{fr} from Eq. (24).
	for each candidate automation plan **do**
	Calculate the relative fitness ratio fr_i using Eq. (25).
	Estimate the solution temperature from the inverse objective value using Eq. (22).
	Generate a trial candidate through the BBSO movement operator in Eq. (26).
	Apply boundary control, binary conversion, and feasibility repair using Eqs. (27) and (28).
	Recalculate reliability indices and the objective-function value using Eq. (21).
	Accept the trial candidate if it improves or preserves fitness according to Eq. (29).
	end for
	Merge the current and trial populations.
	Sort all candidates and retain the best-performing automation plans.
	Update the population size using Eq. (33), if population reduction is activated.
	Update $X_{\rm best}$ using Eq. (30).
	Iter $\leftarrow$ Iter + 1.
	end while
	Return $X_{\rm best}$ and its corresponding device locations, reliability indices, and costs.
	End Procedure.

The full BBSO-based solution workflow, shown in Fig. 3, can be described as follows. First, the candidate locations for reclosers and sectionalizers are defined from the feeder topology. Second, an initial population of feasible automation plans is generated and repaired if necessary. Third, the reliability indices, undelivered energy, and equipment investment cost are calculated for each individual under the considered climatic scenario. Fourth, the objective-function value is evaluated and the population is ranked. Fifth, the BBSO movement operator in (26) generates new candidate automation plans, followed by boundary control, binary mapping, and feasibility repair. Sixth, the acceptance rule in Eq. (29) and the best-solution update in Eq. (30) are applied. Finally, the population-reduction mechanism in Eq. (33) is used to retain the most promising candidates until the stopping condition in Eq. (34) is satisfied.

In the proposed automation-planning application, the best individual obtained by BBSO determines the final placement of reclosers and sectionalizers. Once this placement is identified, the resulting reliability indices and cost terms are recalculated and compared with those obtained from MTBO, CVSO, and TFWO. The detailed mathematical relations in Eqs. (19) to (34).

To assess the robustness and comparative performance of the proposed solution method, three additional population-based metaheuristic algorithms are employed for validation purposes: Mountaineering Team-Based Optimization (MTBO) [22], Corona Virus Search Optimizer (CVSO) [23], Turbulent Flow of Water-Based Optimization (TFWO) [24] All algorithms are implemented under identical population sizes, iteration limits, and stopping criteria.

4. Results and Discussion

The proposed discrete automation-planning problem was solved using four population-based metaheuristic algorithms: BBSO, MTBO, CVSO, and TFWO. To maintain a fair computational comparison, all algorithms were implemented with an identical population size of 50 individuals, a maximum of 30 iterations, the same objective function, the same decision-variable encoding, and the same constraint-handling and feasibility-repair procedures. The algorithm-specific parameters were fixed according to their standard configurations and were not tuned separately for individual scenarios or test networks. Fig. 4 presents the convergence behaviour under Scenario 3, which represents the most demanding planning condition and therefore provides a clearer basis for observing differences in the search dynamics of the compared algorithms.

The detailed statistical validation of the metaheuristic comparison is reported in Appendix B. In that appendix, BBSO, MTBO, CVSO, and TFWO are evaluated over 30 independent runs for each climatic scenario under the same population size, iteration limit, objective function, encoding structure, constraint handling, and repair mechanism. The appendix includes run-by-run objective-function values, summary statistics, CPU-time statistics, and Wilcoxon signed-rank tests. These results show that the superiority of BBSO is not based on a single execution and remains statistically significant at the 5% level.

To validate the proposed model, three distribution systems were considered. The first system is a real medium-voltage feeder from Ardabil Province, namely Feeder 5 of the 63 kV sub-distribution substation located in Khalkhal County. This feeder was selected because it is long, radial, climate-exposed, and representative of the reliability problems faced by mountainous distribution networks in the region. The second system is the IEEE 33-bus benchmark distribution network, whose standard topology is based on the widely used [25] . The third system is the IEEE 69-bus distribution network, adopted from [26], which is used as an additional scalability case to examine the behaviour of the proposed framework under a larger benchmark topology. The topology of the IEEE 33-bus system and IEEE 69-bus system is shown in Fig. 5, the topology of Feeder 5 is provided in Fig. C.1 in Appendix C.

The equipment costs and electricity tariffs were determined according to the meter-tariff guidelines of APED Co. and the relevant Iranian electrical installation standards.

For all test systems, the remaining algorithmic settings, simulation configurations, protective-device price data, tariff assumptions, and modelling parameters are provided in Appendix D. A constant equipment failure rate of 0.6 was used for all buses, allowing the comparative analysis to focus on the effect of coordinated sectionalizer and recloser placement under the three climate-driven operating scenarios.

The optimization analysis for Feeder 5 was performed under three climate-driven operational scenarios that reflect the weather-dependent reliability conditions of Ardabil Province, particularly the Khalkhal feeder area. Since climatic conditions in this mountainous region strongly affect fault occurrence, feeder accessibility, switching delay, and restoration time, the scenarios were defined as operational weather classes rather than general climatic descriptions [27, 28]. For this analysis, the maximum budget constraint was relaxed to identify the best achievable automation plan under investment-unconstrained conditions and to isolate the reliability benefit of coordinated recloser and sectionalizer placement.

Scenario 1, Normal Climate Condition, represents typical non-extreme operation with moderate weather, normal field access, and fault rates and restoration times close to average operating values. Scenario 2, Cold and Snowy Condition, represents winter operation with low temperature, snowfall, increased exposure to weather-related faults, slower crew access, and longer restoration duration. Scenario 3, Severe Winter Condition, represents adverse winter operation in mountainous sections of Ardabil Province, where prolonged cold, icing, heavy snowfall, and accessibility limitations substantially increase fault occurrence, repair time, and reliability risk. The corresponding parameter-extraction logic is summarized in Table 2.

4.1. Planning of a real-scale feeder 5 distribution network

Table 3 quantitatively compares the performance of the four metaheuristic algorithms for Feeder 5 under three climate-driven operational scenarios. The comparison is based on reliability indices, undelivered energy cost, protective equipment investment, and the aggregated objective-function value.

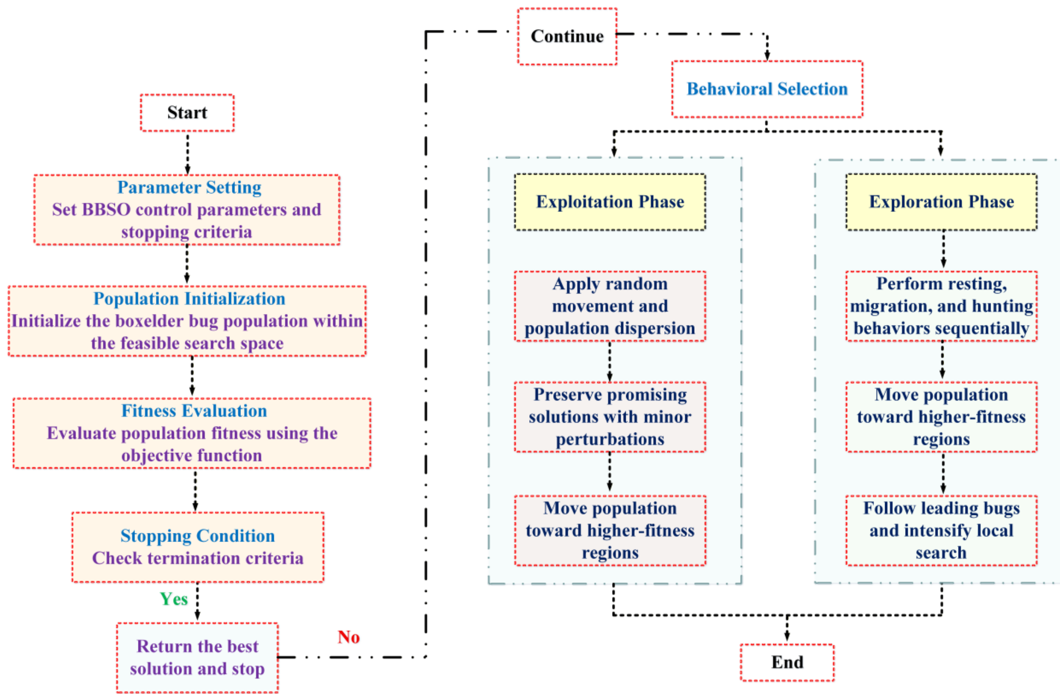

Fig. 3. Flowchart of the proposed population-based optimization framework.

Table 2. Climate-scenario definition and parameter-extraction logic for the Khalkhal feeder.

Scenario	Khalkhal-based climatic interpretation	Operating implication for feeder 5	Parameter-extraction basis
Scenario 1	Normal non-extreme condition outside severe winter periods.	Routine feeder operation, normal road access, ordinary switching conditions, and restoration times close to the annual operating average.	Non-extreme-period values of fault rate, outage duration, and switching time, extracted from utility outage records and normal-operation repair reports.
Scenario 2	Cold and snowy winter condition typical of Khalkhal and Ardabil mountainous operation.	Higher exposure of overhead feeder sections to snow-related faults, slower crew movement, delayed manual switching, and longer restoration duration.	Winter-period utility records, repair reports during snowfall and low-temperature periods, and operator experience for cold-season access and switching delays.
Scenario 3	Severe winter condition with prolonged cold, icing, heavy snowfall, and restricted access to mountainous feeder sections.	Highest reliability stress, increased fault occurrence, extended repair time, delayed fault localization, and larger interruption impact in radial feeder sections.	Severe-event outage records, adverse winter repair reports, and upper-bound utility judgement for fault rate, outage duration, and switching time under inaccessible or partially accessible feeder conditions.

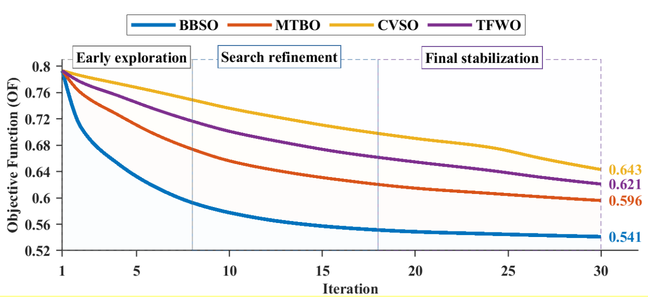

Fig. 4. Convergence behaviour of BBSO, MTBO, CVSO, and TFWO under Scenario 3.

In Scenario 1, the proposed BBSO algorithm reduces SAIFI by approximately 10.1%, 15.1%, and 13.0% compared with MTBO, CVSO, and TFWO, respectively. A similar trend is observed for SAIDI, where BBSO achieves reductions of 8.6% relative to MTBO and more than 12% relative to CVSO. The improvement in MAIFI is more pronounced, with BBSO lowering momentary interruptions by 12.6% compared with MTBO and 18.7% compared with CVSO. These improvements are achieved while maintaining a comparable investment cost, indicating that the superior performance of BBSO is not driven by excessive deployment of protective devices but rather by more effective placement of reclosers and sectionalizers.

Under Scenario 2, which reflects cold and snowy operating conditions, the benefits of optimized protection placement become clearer. BBSO reduces MAIFI by approximately 16.0% relative to MTBO and 24.2% relative to CVSO, highlighting its effectiveness in mitigating short-duration interruptions commonly associated with weather-induced transient faults. SAIFI and SAIDI are also reduced by more than 9% and 8%, respectively, compared with MTBO. These gains result from a more balanced allocation of reclosers and sectionalizers, where reclosers are positioned to isolate transient faults efficiently while sectionalizers limit the propagation of permanent outages without unnecessary redundancy.

Scenario 3 represents the most severe climatic condition and therefore constitutes the most critical planning case. In this scenario, BBSO achieves the lowest objective-function value, improving OF by approximately 9.2% compared with MTBO, 15.9% compared with CVSO, and 12.9% compared with TFWO. SAIFI is reduced by 9.4% relative to MTBO and 15.5% relative to CVSO, while MAIFI shows the most substantial improvement, decreasing by 19.6% and 33.0%, respectively. Although the investment cost for protective equipment is higher in Scenario 3, the reduction in undelivered energy cost offsets this increase, resulting in a net improvement in overall system performance.

The optimized placement for Scenario 3 is illustrated in Fig. 6, where the coordinated deployment of reclosers and sectionalizers

Table 3. Feeder 5 planning results under three climate-driven scenarios.

Scenario	Algorithm	SAIFI (int/cust·yr)	SAIDI (h/cust·yr)	MAIFI (int/cust·yr)	E_{cost} (USD)	Cost (recloser and sectionalizer) (USD)	Objective function (OF)
1	BBSO	0.214	6.05	31.8	48,900	14,500	0.684
	MTBO	0.238	6.62	36.4	52,300	14,200	0.742
	CVSO	0.251	6.88	39.1	55,100	13,900	0.781
	TFWO	0.246	6.71	37.9	53,800	14,000	0.765
2	BBSO	0.187	5.41	22.6	41,200	16,800	0.602
	MTBO	0.206	5.88	26.9	44,900	16,300	0.658
	CVSO	0.219	6.12	29.8	47,600	15,900	0.701
	TFWO	0.213	5.97	28.4	46,100	16,100	0.689
3	BBSO	0.164	5.08	15.2	36,700	19,600	0.541
	MTBO	0.181	5.46	18.9	40,900	18,900	0.596
	CVSO	0.194	5.78	22.7	44,300	18,200	0.643
	TFWO	0.189	5.63	20.8	42,500	18,500	0.621

Table 4. IEEE 33-bus system: reliability indices, cost components, and objective-function values.

Scenario	Algorithm	SAIFI (int/cust·yr)	SAIDI (h/cust·yr)	MAIFI (int/cust·yr)	E_{cost} (USD)	Cost (recloser and sectionalizer) (USD)	Objective function (OF)
1	BBSO	0.2284	6.71	43.24	71,166	11,833	0.742
	MTBO	0.2419	7.08	47.85	75,920	11,500	0.801
	CVSO	0.2567	7.44	52.31	79,480	11,300	0.842
	TFWO	0.2492	7.26	49.68	77,360	11,400	0.821
2	BBSO	0.1685	5.47	22.31	60,666	17,666	0.658
	MTBO	0.1834	5.91	26.84	65,430	17,200	0.712
	CVSO	0.1976	6.24	30.72	69,180	16,900	0.754
	TFWO	0.1918	6.07	28.96	67,250	17,050	0.736
3	BBSO	0.1631	5.24	14.41	57,000	20,666	0.612
	MTBO	0.1798	5.66	18.92	62,480	19,900	0.671
	CVSO	0.1954	6.01	22.84	67,910	19,200	0.726
	TFWO	0.1886	5.83	20.37	65,140	19,600	0.703

Table 5. IEEE 33-bus system: optimal placement of sectionalizers and reclosers across algorithms.

Scenario	Algorithm	Sectionalizers (No.)	Sectionalizer bus(es)	Reclosers (No.)	Recloser bus(es)
1	BBSO	2	16, 7	1	4
	MTBO	2	14, 9	1	5
	CVSO	2	11, 18	1	6
	TFWO	2	13, 8	1	5
2	BBSO	2	6, 5	2	3, 23
	MTBO	2	7, 10	2	4, 22
	CVSO	2	9, 12	2	5, 24
	TFWO	2	8, 11	2	4, 21
3	BBSO	3	23, 7, 2	2	1, 6
	MTBO	3	21, 8, 4	2	2, 7
	CVSO	3	18, 11, 5	2	3, 9
	TFWO	3	20, 10, 6	2	2, 8

strengthens feeder segmentation and fault isolation capability. Reclosers are positioned to address high fault exposure along main feeder sections, enabling rapid restoration following transient faults, while sectionalizers are strategically installed to confine permanent outages to smaller feeder segments. This coordinated placement strategy explains the significant reductions observed in both interruption frequency and duration.

Overall, the results demonstrate that the superiority of BBSO arises not from installing a larger number of protective devices, but from achieving a more effective spatial coordination between reclosers and sectionalizers. By tailoring device placement to fault characteristics and climatic stress levels, BBSO consistently delivers better reliability outcomes and lower composite objective-function values across all scenarios.

From a blackout-scheduling perspective, the placement pattern in Fig. 5 shows how the optimized devices divide Feeder 5 into smaller interruption zones. The upstream reclosers provide faster isolation and reclosing for transient faults, while the sectionalizers confine permanent faults to downstream segments and reduce the number of customers affected by each interruption. Therefore, the reduction in SAIFI, SAIDI, MAIFI, and undelivered energy is not only an algorithmic improvement; it reflects a more effective feeder-level blackout confinement and restoration plan.

4.2. Scalability analysis

A) IEEE 33-bus system distribution network

This subsection investigates the scalability of the proposed optimization framework by applying it to the IEEE 33-bus benchmark distribution network. The analysis focuses on how increasing automation levels, achieved through coordinated placement of reclosers and sectionalizers, affect system reliability and economic performance across multiple metaheuristic solvers.

As shown in Table 4, the proposed BBSO algorithm consistently outperforms MTBO, CVSO, and TFWO across all three scenarios. In Scenario 1, BBSO reduces SAIFI by approximately 5.6%, 11.0%, and 8.3% compared with MTBO, CVSO, and TFWO, respectively. Corresponding reductions in SAIDI range between 5.2% and 9.8%, while MAIFI is lowered by up to 17.3% relative to CVSO. These improvements are achieved without increasing investment cost, indicating more effective utilization of a limited number of protective devices.

Table 6. Computational burden and numerical settings of the metaheuristic algorithms.

Algorithm	Population size	Iterations	Total runtime (s)	Avg. runtime per scenario (s)	Avg. runtime per iteration (s)
BBSO	50	30	132.4	44.1	1.47
MTBO	50	30	146.8	48.9	1.63
CVSO	50	30	161.3	53.8	1.79
TFWO	50	30	154.6	51.5	1.72

Note: All algorithms were executed using identical population size, iteration limits, and scenario definitions. Runtime values represent the average wall-clock time across three climate-driven scenarios.

Table 7. Sensitivity analysis of objective-function weights for Feeder 5 under Scenario 3.

Case	Perturbed priority	w_{EUE}	w_{SAIDI}	w_{SAIFI}	w_{MAIFI}	w_{Ceq}	SAIFI	SAIDI	MAIFI	E_{cost} (USD)	Equipment cost (USD)	(OF)
Baseline	None	0.250	0.250	0.200	0.150	0.150	0.164	5.08	15.2	36,700	19,600	0.541
S1	EUE +20%	0.300	0.233	0.187	0.140	0.140	0.162	5.04	15.0	35,900	20,000	0.536
S2	EUE –20%	0.200	0.267	0.213	0.160	0.160	0.166	5.13	15.5	37,600	19,100	0.548
S3	SAIDI +20%	0.233	0.300	0.187	0.140	0.140	0.163	4.98	15.1	36,200	20,100	0.537
S4	SAIDI –20%	0.267	0.200	0.213	0.160	0.160	0.166	5.19	15.6	37,300	19,000	0.550
S5	SAIFI +20%	0.238	0.238	0.240	0.143	0.143	0.158	5.09	15.1	36,800	20,000	0.538
S6	SAIFI –20%	0.263	0.263	0.160	0.158	0.158	0.171	5.10	15.4	37,100	18,900	0.549
S7	MAIFI +20%	0.241	0.241	0.193	0.180	0.145	0.163	5.07	14.5	36,600	20,000	0.537
S8	MAIFI –20%	0.259	0.259	0.207	0.120	0.155	0.166	5.12	16.0	37,200	19,100	0.548
S9	Cost +20%	0.241	0.241	0.193	0.145	0.180	0.169	5.18	15.8	38,000	18,400	0.553
S10	Cost –20%	0.259	0.259	0.207	0.155	0.120	0.160	5.01	14.8	36,100	20,400	0.535

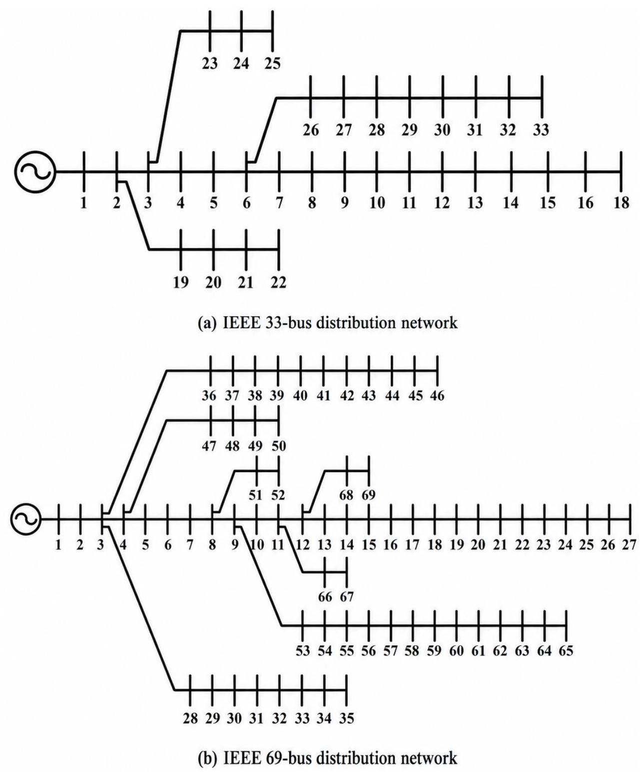

Fig. 5. Benchmark radial distribution networks used for scalability validation: (a) IEEE 33-bus system and (b) IEEE 69-bus system.

In Scenario 2, where automation is expanded through additional reclosers, BBSO achieves further reliability gains. Compared with MTBO, SAIFI and SAIDI decrease by 8.1% and 7.4%, respectively, while MAIFI is reduced by 16.9%. Relative to CVSO, MAIFI improvement exceeds 27.4%, demonstrating BBSO's superior capability in mitigating transient interruptions. Despite comparable equipment costs, BBSO lowers the undelivered energy cost by approximately 7.3%–12.3% compared with the benchmark algorithms.

Scenario 3 represents the highest automation level and the most demanding reliability requirement. In this scenario, BBSO achieves the lowest objective-function value, improving OF by 8.8%, 15.7%, and 12.9% compared with MTBO, CVSO, and TFWO, respectively. SAIFI and SAIDI are reduced by more than 9% relative to MTBO, while MAIFI shows a substantial reduction of 23.8% compared with TFWO and 36.9% compared with CVSO. Although the equipment investment cost is higher, the reduction in undelivered energy cost offsets this increase, resulting in the lowest total system cost among all algorithms.

The placement patterns reported in Table 5 explain these improvements. BBSO consistently positions reclosers closer to the feeder origin and along critical upstream branches, which significantly enhances transient fault clearing and reduces MAIFI. Sectionalizers are strategically distributed across downstream laterals to confine permanent faults to smaller network segments, thereby reducing both interruption frequency and duration. Competing algorithms exhibit less coordinated placement, leading to weaker segmentation and higher residual interruption indices.

Overall, the IEEE 33-bus results confirm the scalability of the proposed approach. As network size and complexity increase, BBSO maintains superior performance by effectively coordinating the number and placement of reclosers and sectionalizers, achieving a robust balance between reliability enhancement and economic efficiency.

B) IEEE 69-bus system distribution network

To further evaluate the scalability of the proposed automation-planning framework, the IEEE 69-bus distribution network was used as a third validation case, in addition to the real Khalkhal feeder and the IEEE 33-bus benchmark network. The aim of this case is to examine whether the reliability-driven placement logic remains effective when the number of candidate buses, lateral branches, and feasible device-location combinations increases. The detailed numerical results for this system are reported in Appendix E. Table E.1 presents the reliability indices, interruption-cost components, equipment costs, and objective-function values; Table E.2 reports the optimal sectionalizer and recloser locations; and Table E.3 summarizes the relative improvements obtained by BBSO over the competing algorithms.

The IEEE 69-bus results confirm the same performance trend observed in the previous two networks. Under Scenario 1, BBSO obtains the lowest objective-function value, 0.793, while MTBO, CVSO, and TFWO produce 0.856, 0.902, and 0.879, respectively. This corresponds to OF reductions of 7.36%, 12.08%, and 9.78% compared with MTBO, CVSO, and TFWO. Under Scenario 2, where climatic severity and interruption exposure increase, the advantage of BBSO becomes more pronounced. The proposed

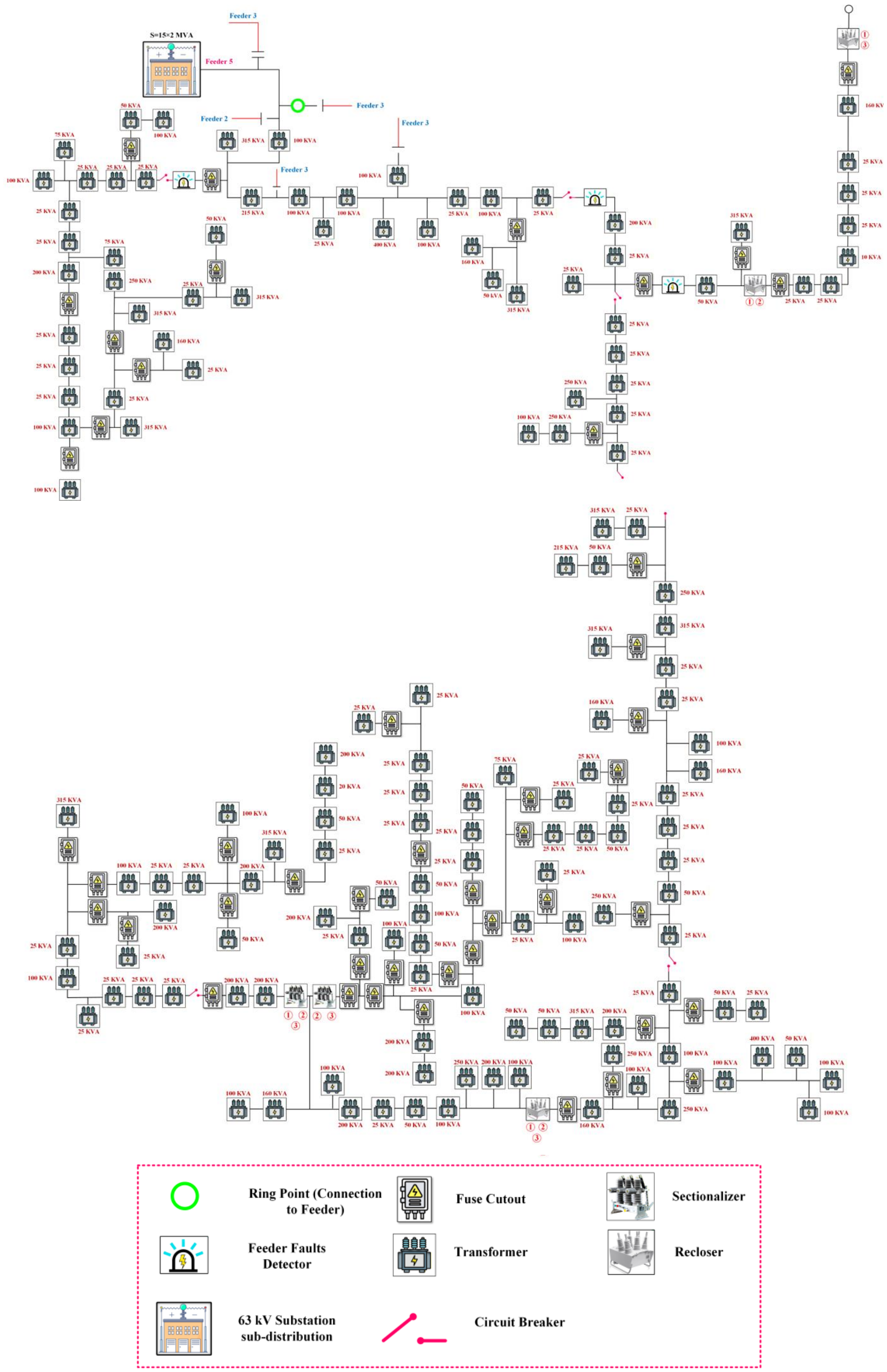

Fig. 6. Optimal placement of reclosers and sectionalizers in Feeder 5 under Scenario 3.

method reduces SAIFI by 8.00% to 15.41%, SAIDI by 7.38% to 12.71%, MAIFI by 14.51% to 25.97%, and Ecost by 7.38% to 13.42% relative to the alternative algorithms.

Scenario 3 provides the most demanding planning condition. In this case, BBSO achieves an objective-function value of 0.651, compared with 0.721 for MTBO, 0.783 for CVSO, and 0.752 for TFWO. The corresponding OF reductions are 9.71%, 16.86%, and 13.43%. Reliability improvements are also substantial: BBSO reduces SAIFI by up to 16.65%, SAIDI by up to 13.22%, MAIFI by up to 37.94%, and Ecost by up to 17.35%. These results indicate that the proposed method is not limited to small benchmark systems. Rather, it preserves its reliability-cost advantage as the network size and placement complexity increase.

4.3. Computational burden and performance assessment

The optimization problem is solved using a population-based metaheuristic framework. Four algorithms, namely BBSO, MTBO, CVSO, and TFWO, are employed under identical computational settings to ensure a fair comparison.

The computational burden is evaluated in terms of total execution time, average runtime per scenario, and convergence efficiency. All simulations were executed sequentially on a standard workstation. Since the solution process relies solely on iterative fitness evaluations and population evolution, no external mathematical solvers are involved.

As summarized in Table 6, BBSO exhibits the lowest computational burden among the compared algorithms while maintaining superior convergence stability. Compared with MTBO, CVSO, and TFWO, BBSO reduces total runtime by approximately 9–18%, indicating more efficient search dynamics. Sensitivity analysis with respect to scenario count shows near-linear growth in runtime for all algorithms; however, BBSO demonstrates the smallest increase, confirming better scalability for multi-scenario planning problems. Importantly, the improved solution quality achieved by BBSO is not accompanied by additional computational cost, highlighting its suitability for reliability-oriented distribution network planning.

4.4. Sensitivity analysis

A sensitivity analysis was carried out to examine whether the planning results depend strongly on the selected weighting coefficients. The analysis was performed for Feeder 5 under Scenario 3, because this case represents the most severe climatic condition and the most demanding planning situation in the real feeder. Starting from the baseline weight vector, each coefficient was individually increased and decreased by 20%. When one coefficient was perturbed, the remaining coefficients were rescaled proportionally so that the sum of all weights remained equal to one. For a perturbed coefficient w_i, the remaining coefficients were adjusted as $w'_j = w_j\left(1 - w'_i\right) / \left(1 - w_i\right),\ j \neq i$. This procedure isolates the effect of each planning priority without changing the total weight assigned to the objective function.

Table 7 reports the numerical sensitivity results. The baseline case corresponds to the BBSO solution for Feeder 5 under Scenario 3. Increasing the weights assigned to EUE and SAIDI slightly improves undelivered-energy cost and outage duration, respectively, although this requires a small increase in equipment investment. A higher SAIFI weight shifts the solution toward lower interruption frequency, while a higher MAIFI weight improves momentary-interruption performance. Conversely, increasing the equipment-cost weight produces a more conservative placement pattern, with lower investment cost but slightly weaker reliability indices. Across all perturbation cases, the objective-function value remains within a narrow range around the baseline value, indicating that the proposed planning decision is not driven by a single coefficient. The ranking of BBSO as the best-performing algorithm also remains unchanged. The sensitivity results show that the proposed formulation has stable behaviour under moderate variations in the weighting coefficients. The maximum deviation of the objective-function value from the baseline case is limited to 2.2%, which occurs when the equipment-cost weight is increased. This case intentionally penalizes investment more strongly and therefore produces a lower-cost but less reliability-oriented placement.

5. CONCLUSION

This work proposes an approach for the optimal scheduling of distributed generators (DGs) in a microgrid that includes residential, industrial, and commercial voltage-dependent loads, which fluctuate across different seasons. The Shuffled BAT Optimization Algorithm (SBOA) is utilized to establish the most efficient schedules, aiming to minimize losses, voltage variations, and generating costs. This approach ensures reliable load fulfillment, as measured by the reliability index EIR. The approach is evaluated on the modified 33-bus radial distribution system, considered as an MMG system with three microgrids. Additionally, the influence of demand response (DR) initiatives on optimal day-ahead scheduling in a microgrid with various renewable energy sources (RES) is investigated. Three DR-based scenarios—without DRPs, with Time-of-Use (TOU) pricing, and with Real-Time Pricing (RTP)—are studied. In the case without DRP, based on the Mean, the cost function optimized with PSO achieves a better global optimum value of about \$1974.07/hr. Compared to stochastic optimization, PSO yields a global optimum value and reduces the price reduction by 1.05%. With DRPs, based on the standard deviation, the optimal value of the cost function was obtained using PSO and stochastic optimization as \$73.45/hr and \$96.17/hr for TOU, respectively. Comparing PSO with stochastic optimization for TOU based on standard deviation, PSO achieves a better price reduction of 30.5% than stochastic optimization. For RTP, based on standard deviation, PSO demonstrates better optimal performance, with a 15.9% improvement over stochastic optimization. The results illustrate the significant benefits of DRPs in multi-microgrids, particularly in reducing costs for both power suppliers and consumers by flattening the demand curve. The Particle Swarm Optimization (PSO) algorithm effectively addresses the issues of optimal microgrid scheduling, even with uncertain parameters, proving its advantages over stochastic optimization methods. Furthermore, the Jaya algorithm, a novel metaheuristic optimization technique, is employed to optimize single and multi-objective functions, such as lowering operational expenses, system losses, and voltage deviations, on a modified 33-bus distribution system. The results obtained using the Jaya algorithm are compared with those obtained using the Genetic Algorithm (GA), showing an operational cost of about \$178,158.36/hr, power losses of 56.15 kW, and voltage deviations of 1.05E-03. Comparing these results with GA, the superiority of the Jaya algorithm is evident, as it achieves minimal operating costs, system losses, and voltage deviations. The Jaya algorithm reduces the operational cost of the multi-microgrid by about 16.4% compared to GA, with power losses being 20.7% lower than GA.

The proposed strategy can result in inaccurate load predictions, which may lead to inefficient scheduling, potentially increasing operating expenses or compromising system reliability. Due to uncertainties, robust optimization methods are required, which add complexity to the task. As the number of microgrids and distributed generation systems (DGs) increases, the optimization model becomes more complex and more challenging to solve. Many algorithms face challenges in achieving efficient scalability, which limits their application in large-scale MMG systems.

To address these issues, future work should explore hybrid methodologies that integrate heuristic techniques, such as greedy algorithms, with metaheuristics, such as genetic algorithms, to achieve a balance between solution quality and computational efficiency. These approaches could be customized to provide faster convergence while still obtaining solutions that are close to optimal. For load forecasting, stochastic optimization methods that consider uncertainty in both renewable generation and load estimates should be utilized. These techniques can improve scheduling efficiency in various scenarios, enhancing resilience to unexpected changes.

ACKNOWLEDGEMENT

The authors acknowledge the use of artificial intelligence tools (e.g., ChatGPT by OpenAI) for language editing and clarity improvement during the preparation of this manuscript. The authors are fully responsible for the scientific content, analysis, and conclusions.

APPENDIX

APPENDIX A: MATHEMATICAL NOTATION (TABLE A.1)

Table A.1. Mathematical notation.

Notation	Description	Unit
	Indices	
i	Index representing a candidate installation location for protective devices	–
k	Index denoting a load point or customer aggregation node	–
l	Index corresponding to a distribution line or feeder segment	–
t	Index of time period or operating interval	–
	Sets	
$\mathcal{L}$	Set of all distribution lines in the network	–
$\mathcal{K}$	Set of load points or customer locations	–
$\mathcal{I}$	Set of feasible candidate locations for installing protection devices	–
	Parameters	
C_{inv}	Total investment cost associated with installed protective equipment	USD
C_R	Unit procurement and installation cost of a recloser	USD
C_S	Unit procurement and installation cost of a sectionalizer	USD
$B_{\max}$	Maximum allowable budget for automation investment	USD
E_{UE}	Expected undelivered electrical energy over the planning horizon	kWh
N_k	Number of customers connected at load point k	customers
P_l	Electrical load supplied by line l	kW
SAIDI	System Average Interruption Duration Index	h/cust·yr
SAIFI	System Average Interruption Frequency Index	int/cust·yr
MAIFI	Momentary Average Interruption Frequency Index	int/cust·yr
r_k	Average interruption duration experienced at load point k	h
r_l	Average outage duration of line l following a fault	h
λ_l	Failure rate associated with line l	faults/yr
λ_k^m	Transient fault rate contributing to momentary interruptions at load point k	faults/yr
w_i	Weighting coefficient assigned to objective-function component i	–
a	Lower bound of a fuzzy parameter	–
b	Most probable value of a fuzzy parameter	–
c	Upper bound of a fuzzy parameter	–
	Decision Variables	
x_i	Binary variable indicating installation of a protective device at location i (1 if installed, 0 otherwise)	–
N_R	Number of reclosers installed in the network	–
N_S	Number of sectionalizers installed in the network	–
$\tilde{x}$	Defuzzified crisp value of a fuzzy decision or parameter	–

APPENDIX B: STATISTICAL VALIDATION OF METAHEURISTIC ALGORITHMS

Appendix B reports the statistical validation of the compared stochastic metaheuristic algorithms. Each algorithm was implemented under the same objective function, decision-variable encoding, constraint-handling strategy, feasibility-repair procedure, population size, iteration limit, and stopping criterion. Thirty independent runs were considered for each algorithm and scenario. The final objective-function value of each run was retained for statistical analysis. Lower objective-function values indicate better solutions.

Table B.1. Statistical implementation protocol used for algorithm comparison.

Item	Setting used in the statistical validation
Compared algorithms	BBSO, MTBO, CVSO, and TFWO
Number of independent runs	30 runs for each algorithm and scenario
Population size	50 individuals
Maximum iterations	30 iterations
Objective function	Same normalized reliability–cost objective function
Constraint handling	Same feasibility-repair procedure
Statistical test	Wilcoxon signed-rank test, $\alpha = 0.05$
Performance direction	Lower OF is better

Table B.2. Run-by-run final objective-function values for Scenario 1.

Run	BBSO	MTBO	CVSO	TFWO	Best algorithm
1	0.6967	0.7484	0.8094	0.7753	BBSO
2	0.6896	0.7535	0.7954	0.7829	BBSO
3	0.6905	0.7610	0.8052	0.7670	BBSO
4	0.6938	0.7704	0.8122	0.7650	BBSO
5	0.6925	0.7668	0.8167	0.7766	BBSO
6	0.6916	0.7642	0.8088	0.7796	BBSO
7	0.6840	0.7495	0.7830	0.8078	BBSO
8	0.6980	0.7733	0.8225	0.7908	BBSO
9	0.6957	0.7584	0.7810	0.7902	BBSO
10	0.6983	0.7665	0.8113	0.7830	BBSO
11	0.6895	0.7661	0.8213	0.7745	BBSO
12	0.6910	0.7682	0.8079	0.7747	BBSO
13	0.6886	0.7507	0.8023	0.7780	BBSO
14	0.6880	0.7580	0.8018	0.8078	BBSO
15	0.7032	0.7553	0.8039	0.7775	BBSO
16	0.6902	0.7539	0.8030	0.7944	BBSO
17	0.6865	0.7562	0.8202	0.7917	BBSO
18	0.6950	0.7553	0.8109	0.7827	BBSO
19	0.6952	0.7645	0.8099	0.7900	BBSO
20	0.6924	0.7561	0.8047	0.7882	BBSO
21	0.7018	0.7624	0.7848	0.7740	BBSO
22	0.6958	0.7523	0.7978	0.7805	BBSO
23	0.6946	0.7673	0.7855	0.7727	BBSO
24	0.6887	0.7765	0.7922	0.7698	BBSO
25	0.6897	0.7626	0.8072	0.7897	BBSO
26	0.6888	0.7463	0.8078	0.8000	BBSO
27	0.6981	0.7778	0.7924	0.7908	BBSO
28	0.6958	0.7420	0.8077	0.7944	BBSO
29	0.6910	0.7689	0.7885	0.7721	BBSO
30	0.6860	0.7584	0.7830	0.8026	BBSO

Table B.3. Run-by-run final objective-function values for Scenario 2.

Run	BBSO	MTBO	CVSO	TFWO	Best algorithm
1	0.6114	0.6600	0.7058	0.6988	BBSO
2	0.6174	0.6763	0.7422	0.7196	BBSO
3	0.6092	0.6726	0.7106	0.6968	BBSO
4	0.6109	0.6809	0.7508	0.6910	BBSO
5	0.6152	0.6740	0.7087	0.7086	BBSO
6	0.6062	0.6902	0.7350	0.7097	BBSO
7	0.6056	0.6812	0.7362	0.7032	BBSO
8	0.6113	0.6630	0.7292	0.7026	BBSO
9	0.6056	0.6580	0.7311	0.7128	BBSO
10	0.6141	0.6810	0.7444	0.7136	BBSO
11	0.6150	0.6789	0.7160	0.7274	BBSO
12	0.6070	0.6992	0.7419	0.6986	BBSO
13	0.6020	0.6692	0.7252	0.7273	BBSO
14	0.6093	0.6992	0.7201	0.6964	BBSO
15	0.6105	0.6609	0.7201	0.6980	BBSO
16	0.6088	0.6600	0.7266	0.7025	BBSO
17	0.6073	0.6600	0.7153	0.7045	BBSO
18	0.6170	0.6872	0.7331	0.6960	BBSO
19	0.6040	0.6715	0.7493	0.7037	BBSO
20	0.6203	0.6819	0.7463	0.7002	BBSO
21	0.6040	0.6760	0.7480	0.6919	BBSO
22	0.6040	0.6856	0.7342	0.6910	BBSO
23	0.6214	0.6911	0.7127	0.7067	BBSO
24	0.6138	0.6786	0.7074	0.7105	BBSO
25	0.6161	0.6618	0.7053	0.7080	BBSO
26	0.6214	0.6758	0.7419	0.6890	BBSO
27	0.6131	0.6888	0.7175	0.6925	BBSO
28	0.6080	0.6694	0.7010	0.7230	BBSO
29	0.6143	0.6777	0.7407	0.6985	BBSO
30	0.6095	0.6719	0.7162	0.7172	BBSO

Table B.4. Run-by-run final objective-function values for Scenario 3.

Run	BBSO	MTBO	CVSO	TFWO	Best algorithm
1	0.5456	0.5980	0.6886	0.6671	BBSO
2	0.5552	0.6198	0.6743	0.6331	BBSO
3	0.5563	0.6112	0.6450	0.6230	BBSO
4	0.5505	0.6189	0.6799	0.6516	BBSO
5	0.5443	0.6056	0.6663	0.6321	BBSO
6	0.5431	0.6015	0.6753	0.6361	BBSO
7	0.5544	0.6083	0.6618	0.6479	BBSO
8	0.5533	0.6185	0.6810	0.6396	BBSO
9	0.5430	0.6268	0.6696	0.6257	BBSO
10	0.5647	0.5980	0.6789	0.6434	BBSO
11	0.5581	0.6314	0.6485	0.6605	BBSO
12	0.5547	0.6256	0.6770	0.6694	BBSO
13	0.5494	0.6153	0.6876	0.6490	BBSO
14	0.5598	0.6051	0.6744	0.6314	BBSO
15	0.5563	0.6143	0.6659	0.6271	BBSO
16	0.5410	0.6076	0.6552	0.6371	BBSO
17	0.5447	0.6161	0.6450	0.6333	BBSO
18	0.5430	0.6120	0.6971	0.6339	BBSO
19	0.5444	0.6173	0.6810	0.6561	BBSO
20	0.5460	0.6294	0.6880	0.6458	BBSO
21	0.5550	0.6357	0.6850	0.6579	BBSO
22	0.5624	0.6236	0.6723	0.6482	BBSO
23	0.5438	0.6152	0.6925	0.6210	BBSO
24	0.5605	0.6332	0.6831	0.6539	BBSO
25	0.5543	0.6186	0.6450	0.6403	BBSO
26	0.5462	0.6042	0.6782	0.6522	BBSO
27	0.5449	0.6268	0.6430	0.6413	BBSO
28	0.5538	0.6107	0.6578	0.6423	BBSO
29	0.5697	0.5960	0.6650	0.6506	BBSO
30	0.5484	0.6128	0.6617	0.6582	BBSO

Table B.5. Summary statistics of final objective-function values over 30 independent runs.

Scenario	Algorithm	Best	Mean	Median	Worst	Std. dev.	IQR	Mean rank	Wins / 30
Scenario 1	BBSO	0.6840	0.6927	0.6920	0.7032	0.0046	0.0062	1.00	30
	MTBO	0.7420	0.7604	0.7597	0.7778	0.0089	0.0125	2.07	0
	CVSO	0.7810	0.8026	0.8049	0.8225	0.0119	0.0166	3.87	0
	TFWO	0.7650	0.7842	0.7828	0.8078	0.0116	0.0160	3.07	0
Scenario 2	BBSO	0.6020	0.6111	0.6107	0.6214	0.0054	0.0077	1.00	30
	MTBO	0.6580	0.6761	0.6761	0.6992	0.0115	0.0125	2.07	0
	CVSO	0.7010	0.7271	0.7279	0.7508	0.0151	0.0261	3.80	0
	TFWO	0.6890	0.7047	0.7029	0.7274	0.0107	0.0132	3.13	0
Scenario 3	BBSO	0.5410	0.5516	0.5519	0.5697	0.0074	0.0112	1.00	30
	MTBO	0.5960	0.6152	0.6153	0.6357	0.0107	0.0149	2.03	0
	CVSO	0.6430	0.6708	0.6744	0.6971	0.0153	0.0193	3.97	0
	TFWO	0.6210	0.6436	0.6429	0.6694	0.0127	0.0186	3.00	0

Table B.6. CPU-time statistics over 30 independent runs.

Scenario	Algorithm	Mean CPU time (s)	Std. dev. (s)	Minimum (s)	Maximum (s)
Scenario 1	BBSO	3.76	0.11	3.46	3.97
	MTBO	3.66	0.16	3.42	4.03
	CVSO	4.01	0.15	3.73	4.35
	TFWO	3.93	0.15	3.59	4.16
Scenario 2	BBSO	4.14	0.18	3.80	4.46
	MTBO	4.03	0.17	3.67	4.36
	CVSO	4.38	0.16	4.14	4.68
	TFWO	4.21	0.18	3.95	4.52
Scenario 3	BBSO	4.60	0.20	4.26	4.95
	MTBO	4.45	0.22	4.12	4.82
	CVSO	4.85	0.21	4.53	5.23
	TFWO	4.73	0.21	4.40	5.10

Table B.7. Pairwise Wilcoxon signed-rank tests between BBSO and competing algorithms.

Scenario	Comparison	Test	W statistic	z value	p-value	Rank-biserial r	Decision at $\alpha = 0.05$
Scenario 1	BBSO vs MTBO	Wilcoxon signed-rank	0	-6.009	< 0.0001	1.000	Significant
	BBSO vs CVSO	Wilcoxon signed-rank	0	-6.009	< 0.0001	1.000	Significant
	BBSO vs TFWO	Wilcoxon signed-rank	0	-6.009	< 0.0001	1.000	Significant
Scenario 2	BBSO vs MTBO	Wilcoxon signed-rank	0	-6.009	< 0.0001	1.000	Significant
	BBSO vs CVSO	Wilcoxon signed-rank	0	-6.009	< 0.0001	1.000	Significant
	BBSO vs TFWO	Wilcoxon signed-rank	0	-6.009	< 0.0001	1.000	Significant
Scenario 3	BBSO vs MTBO	Wilcoxon signed-rank	0	-6.009	< 0.0001	1.000	Significant
	BBSO vs CVSO	Wilcoxon signed-rank	0	-6.009	< 0.0001	1.000	Significant
	BBSO vs TFWO	Wilcoxon signed-rank	0	-6.009	< 0.0001	1.000	Significant

APPENDIX C: DETAILED TOPOLOGY OF THE REAL DISTRIBUTION FEEDER (FIG. C.1)

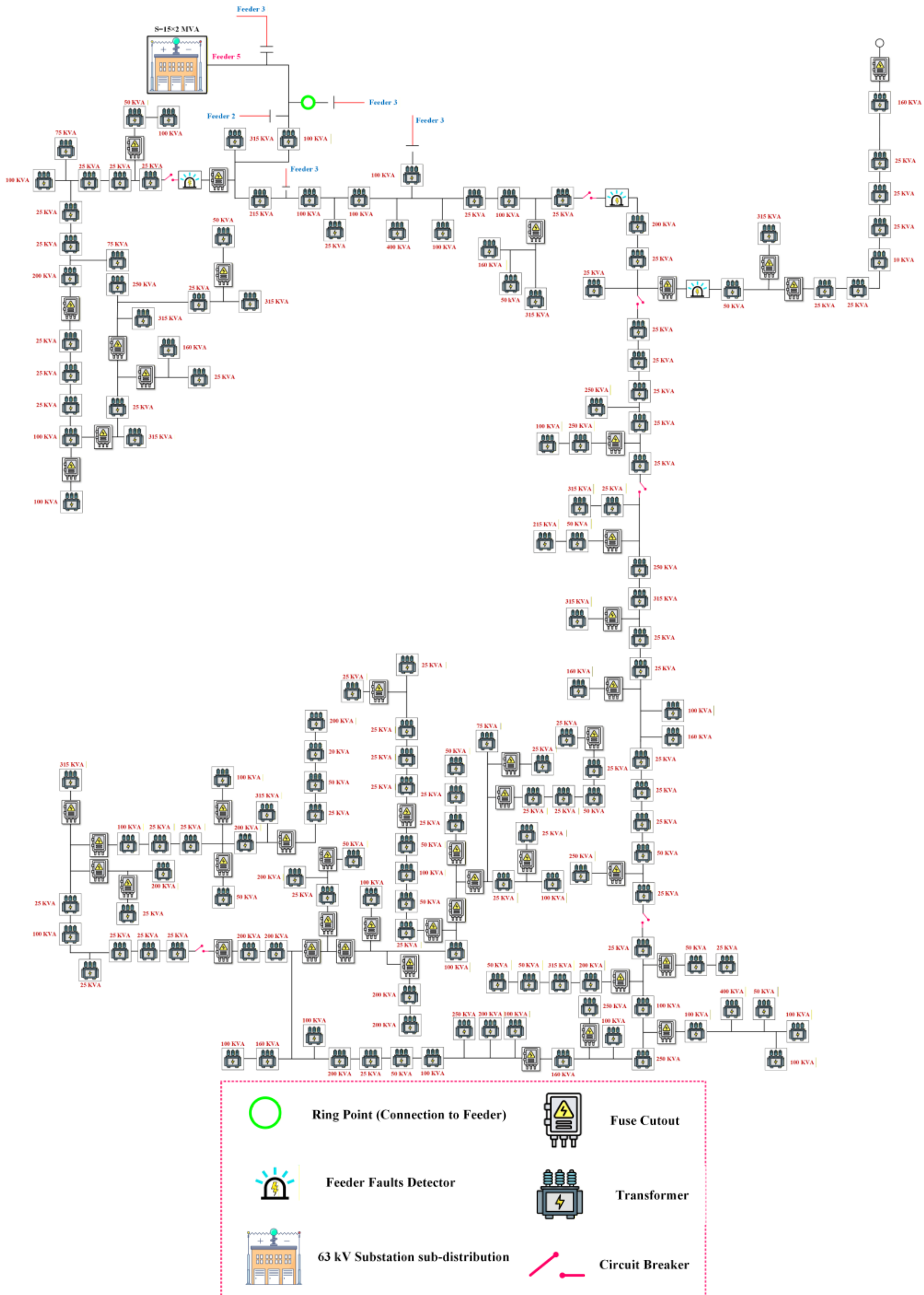

Fig. C.1. Network topology of Feeder 5 in the Ardabil Province electricity distribution system.

APPENDIX D: INPUT DATA AND SIMULATION SETTINGS

Table D.1. Tunable parameters of the BBSO algorithm.

Parameter	Symbol	Description	Value
Exploration probability	P_{exp}	Controls random dispersal during global search	0.30
Exploitation probability	P_{expl}	Regulates intensification around promising regions	0.70
Following coefficient	α	Attraction strength toward leading bugs	0.50
Random deviation factor	β	Stochastic perturbation to avoid local optima	0.20
Survival threshold	τ	Controls population loss and regeneration	0.10

Table D.2. Tunable parameters of the MTBO algorithm.

Parameter	Symbol	Description	Value
Number of teams	N_{team}	Number of mountaineering groups	4
Leader influence factor	λ	Guidance strength of team leaders	0.60
Exploration step size	Δ_{expl}	Step magnitude during uphill exploration	0.25
Cooperation rate	C_r	Information sharing among teams	0.40
Fatigue factor	F_t	Reduction of movement capability	0.10

Table D.3. Tunable Parameters of the CVSO Algorithm.

Parameter	Symbol	Description	Value
Damping coefficient	K_d	Probability of individual death and regeneration	0.10
Number of societies	N_v	Number of virus societies	4
Evolutionary cycles	N_e	Number of evolution steps	5
Social learning factor	ξ	Attraction toward the best virus agent	0.50
Migration ratio	N_t	Proportion of inter-society migration	0.20

Table D.4. Tunable parameters of the TFWO algorithm.

Parameter	Symbol	Description	Value
Number of whirlpools	N_{Wh}	Number of whirlpool groups	4
Centrifugal force threshold	F_E	Escape trigger from local regions	0.50
Angular deviation	δ	Rotational movement around whirlpool	$\pi/4$

Table D.5. IEEE 33-bus system — bus load data.

Bus No.	**Bus type**	**Real power load (MW)**	**Reactive power load (MVAr)**	**Base voltage (kV)**
1	Slack	0.000	0.000	12.66
2	PQ	0.100	0.060	12.66
3	PQ	0.090	0.040	12.66
4	PQ	0.120	0.080	12.66
5	PQ	0.060	0.030	12.66
6	PQ	0.060	0.020	12.66
7	PQ	0.200	0.100	12.66
8	PQ	0.200	0.100	12.66
9	PQ	0.060	0.020	12.66
10	PQ	0.060	0.020	12.66
11	PQ	0.045	0.030	12.66
12	PQ	0.060	0.035	12.66
13	PQ	0.060	0.035	12.66
14	PQ	0.120	0.080	12.66
15	PQ	0.060	0.010	12.66
16	PQ	0.060	0.020	12.66
17	PQ	0.060	0.020	12.66
18	PQ	0.090	0.040	12.66
19	PQ	0.090	0.040	12.66
20	PQ	0.090	0.040	12.66
21	PQ	0.090	0.040	12.66
22	PQ	0.090	0.040	12.66
23	PQ	0.090	0.050	12.66
24	PQ	0.420	0.200	12.66
25	PQ	0.420	0.200	12.66
26	PQ	0.060	0.025	12.66
27	PQ	0.060	0.025	12.66
28	PQ	0.060	0.020	12.66
29	PQ	0.120	0.070	12.66
30	PQ	0.200	0.100	12.66
31	PQ	0.150	0.070	12.66
32	PQ	0.210	0.100	12.66
33	PQ	0.060	0.040	12.66

Table D.6. IEEE 33-Bus System – Line Impedance Data.

From bus	**To bus**	**Resistance (Ω)**	**Reactance (Ω)**
1	2	0.057526	0.029324
2	3	0.307595	0.156668
3	4	0.228357	0.116300
4	5	0.237778	0.121104
5	6	0.510995	0.441115
6	7	0.116799	0.386085
7	8	0.443860	0.146685
8	9	0.642643	0.461705
9	10	0.651378	0.461705
10	11	0.122664	0.040555
11	12	0.233598	0.077242
12	13	0.915922	0.720634
13	14	0.337918	0.444796
14	15	0.338414	0.444496
15	16	0.257454	0.992500
16	17	0.229738	0.939000
17	18	0.740299	0.958923

Table D.7. Data of Feeder 5.

Parameter	**Value**	**Unit**
Feeder voltage level	63 (substation)	kV
Feeder length	534.366	km
Line resistance per km	0.306456	Ω/km
Line reactance per km	0.2464	Ω/km
Protective equipment cost (sectionalizer)	300	USD
Protective equipment cost (recloser)	583.33	USD
Electricity export tariff	0.0276	USD/kWh

Table E.1. IEEE 69-bus system: Reliability indices, cost components, and objective-function values.

Scenario	Algorithm	SAIFI	SAIDI	MAIFI	E_{cost} (USD)	Cost (Recloser and dectionalizer) (USD)	Objective Function (OF)
1	BBSO	0.3126	8.94	58.72	99,860	16,400	0.793
	MTBO	0.3318	9.41	64.55	106,230	15,950	0.856
	CVSO	0.3525	9.88	70.18	112,740	15,700	0.902
	TFWO	0.3441	9.67	67.42	109,580	15,820	0.879
2	BBSO	0.2382	7.28	32.64	84,700	24,600	0.704
	MTBO	0.2589	7.86	38.18	91,450	23,950	0.764
	CVSO	0.2816	8.34	44.09	97,830	23,400	0.814
	TFWO	0.2712	8.09	41.21	95,060	23,700	0.793
3	BBSO	0.2307	6.96	20.38	79,640	28,700	0.651
	MTBO	0.2534	7.54	27.16	88,930	27,900	0.721
	CVSO	0.2768	8.02	32.84	96,360	27,100	0.783
	TFWO	0.2671	7.78	29.45	92,840	27,500	0.752

Table E.2. IEEE 69-bus system: Optimal placement of sectionalizers and reclosers across algorithms.

Scenario	Algorithm	Sectionalizers (No.)	Sectionalizer bus(es)	Reclosers (No.)	Recloser bus(es)
1	BBSO	3	18, 35, 56	1	7
	MTBO	3	16, 39, 61	1	8
	CVSO	3	21, 42, 63	1	9
	TFWO	3	19, 38, 60	1	8
2	BBSO	4	12, 28, 45, 61	2	3, 11
	MTBO	4	14, 31, 47, 63	2	4, 13
	CVSO	4	16, 35, 50, 66	2	5, 15
	TFWO	4	15, 33, 49, 65	2	4, 14
3	BBSO	5	11, 26, 39, 53, 66	3	2, 8, 17
	MTBO	5	13, 28, 42, 56, 67	3	3, 10, 19
	CVSO	5	15, 31, 46, 59, 68	3	4, 12, 21
	TFWO	5	14, 30, 44, 57, 68	3	3, 11, 20

Table E.3. IEEE 69-bus system: relative improvement of BBSO over competing algorithms.

Scenario	Comparator	SAIFI improvement (%)	SAIDI improvement (%)	MAIFI improvement (%)	E_{cost} improvement (%)	OF improvement (%)
1	BBSO vs MTBO	5.79	4.99	9.03	6.00	7.36
	BBSO vs CVSO	11.32	9.51	16.33	11.42	12.08
	BBSO vs TFWO	9.15	7.55	12.90	8.87	9.78
2	BBSO vs MTBO	8.00	7.38	14.51	7.38	7.85
	BBSO vs CVSO	15.41	12.71	25.97	13.42	13.51
	BBSO vs TFWO	12.17	10.01	20.80	10.90	11.22
3	BBSO vs MTBO	8.96	7.69	24.96	10.45	9.71
	BBSO vs CVSO	16.65	13.22	37.94	17.35	16.86
	BBSO vs TFWO	13.63	10.54	30.80	14.22	13.43

Appendix E: IEEE 69-bus system distribution-network results

This appendix reports the detailed numerical results used to support the IEEE 69-bus validation case. The tables include reliability indices, interruption-cost components, objective-function values, optimal placement decisions, and the relative improvement of BBSO with respect to the competing metaheuristic algorithms under the three climatic scenarios.

References

[1] M. Alimohammadi and J. Behnamian, "Preventive maintenance scheduling of electricity distribution network feeders to reduce undistributed energy: A case study in Iran," *Electr. Power Syst. Res.*, vol. 201, p. 107509, 2021.

[2] G. Farshchian, S. A. Darestani, and N. Hamidi, "Developing a decision-making dashboard for power losses attributes of Iran's electricity distribution network," *Energy*, vol. 216, p. 119248, 2021.

[3] A. Arefi, J. Olamaei, A. Yavartalab, and H. Keshtkar, "Loss reduction experiences in electric power distribution companies of Iran," *Energy Procedia*, vol. 14, pp. 1392–1397, 2012.

[4] B. S. Buss, L. M. Carvalho, M. E. P. Monteiro, and D. Issicaba, "A multi-objective cross-entropy approach applied to recloser allocation in distribution systems," *Electr. Power Syst. Res.*, vol. 247, p. 111708, 2025.

[5] L. S. de Assis, G. P. Epifanio, F. L. Usberti, J. F. V. González, and C. Cavellucci, "Evolutionary algorithms for switch allocation in power distribution networks with distributed generation," *Electr. Power Syst. Res.*, vol. 249, p. 112013, 2025.

[6] W. R. Faria, G. Muñoz-Delgado, J. Contreras, and B. R. Pereira, "A novel MILP formulation for optimal allocation and coordination of protective and switching devices in active distribution networks," *Sustain. Energy Grids Netw.*, vol. 42, p. 101692, 2025.

[7] M. Ebrahimi and M. Rastegar, "Optimal planning of fault interrupter and load break switches in power distribution systems: A linear power flow-constrained multi-objective optimization," *Reliab. Eng. Syst. Saf.*, vol. 264, p. 111457, 2025.

[8] M. Sadeghian-Jahromi, M. Fotuhi-Firuzabad, S. Fattaheian-Dehkordi, F. Wang, and M. Lehtonen, "Simultaneous planning of distribution automation and battery energy storage systems for improving resilience of distribution network," *Sustain. Energy Grids Netw.*, vol. 42, p. 101709, 2025.

[9] Z. Huang, D. Xu, X. Yang, H. Yang, Z. Bai, and D. Shi, "Resilient planning of multi-type remote-controlled switches and soft open points in distribution systems under thunderstorm disasters," *Cyber-Phys. Energy Syst.*, vol. 16, pp. 989–1002, 2025.

[10] Z. Esmaeilzadeh, H. Falaghi, and M. Ramezani, "Reliability-oriented AC/DC hybrid distribution network planning: A risk-constrained approach," *Renew. Energy Focus*, vol. 56, p. 100790, 2026.

[11] A. M. Fam, A. Safdarian, M. Fotuhi-Firuzabad, M. Lehtonen, and M. Pourakbari-Kasmaei, "Data envelopment analysis to determine reliability targets for power distribution systems," *Appl. Energy*, vol. 394, p. 126175, 2025.

[12] Z. Wang, T. Yu, P. Fan, and M. Wang, "Topology-variable-based reliability modeling for optimal smart switch deployment in flexible distribution networks with scenario-based parallel progressive hedging algorithm," *Energy Convers. Manag.: X*, vol. 30, p. 101596, 2026.

[13] G. Li, D. Zhang, and Z. Bie, "An analytical method for reliability and resilience evaluation of power distribution systems with mobile power sources," *Reliab. Eng. Syst. Saf.*, vol. 267, p. 111817, 2026.

[14] H. Qi, C. Li, C. Gai, R. Sun, and J. Yan, "Optimization of power system emergency load shedding with surrogate-assisted proliferation-reduction differential evolution algorithm," *Int. J. Electr. Power Energy Syst.*, vol. 173, p. 111358, 2025.

[15] H. Yan, J. Wang, C. Zhang, R. Liu, X. Yuan, and J. Zhao, "Cost-estimation-based restoration of active distribution networks considering differentiated customer reliability demands," *Int. J. Electr. Power Energy Syst.*, vol. 175, p. 111570, 2026.

[16] Z. Wang, H. Hou, C. Liu, S. Wang, Z. Li, X. Lin, *et al.*, "Distribution network gray-start and emergency recovery strategy with pumped storage unit under a typhoon," *Glob. Energy Interconnect.*, vol. 8, pp. 121–133, 2025.

[17] Y. Li, Z. Hu, T. Li, L. Sha, and Z. Zhang, "Flexible scheduling strategy considering multifaceted flexible resources and transmission-distribution network cooperative optimization," *Energy Rep.*, vol. 13, pp. 2892–2906, 2025.

[18] M. A. Farid, I. Nutkani, L. Meegahapola, and N. Fernando, "Protection solutions and their performance assessment for MV embedded microgrid networks," *Renew. Energy Focus*, p. 100819, 2026.

[19] A. Aščerić and M. Čepin, "Improving power distribution system reliability via optimized microgrid integration and storage management," *Reliab. Eng. Syst. Saf.*, p. 111386, 2025.

[20] P. Zare, A. Mohammadian, S. J. SeyedShenava, H. Shayeghi, and I. F. Davoudkhani, "A framework for blackout scheduling and management in Iran's electricity distribution network: A case study of ardabil province electricity distribution company," in *Proc. Int. Electr. Power Distrib. Conf.*, 2024.

[21] I. F. Davoudkhani, H. Shayeghi, and A. Younesi, "Boxelder bug search optimization: A novel reliable tool for optimizing engineering problems through bio-inspired ecology of boxelder bugs," *Neural Comput. Appl.*, vol. 37, pp. 26593–26657, 2025.

[22] I. Faridmehr, M. L. Nehdi, I. F. Davoudkhani, and A. Poolad, "Mountaineering team-based optimization: A novel human-based metaheuristic algorithm," *Mathematics*, vol. 11, p. 1273, 2023.

[23] K. Golalipour, I. F. Davoudkhani, S. Nasri, A. Naderipour, S. Mirjalili, A. Y. Abdelaziz, *et al.*, "The corona virus search optimizer for solving global and engineering optimization problems," *Alex. Eng. J.*, vol. 78, pp. 614–642, 2023.

[24] M. Ghasemi, I. F. Davoudkhani, E. Akbari, A. Rahimnejad, S. Ghavidel, and L. Li, "A novel and effective optimization algorithm for global optimization and its engineering applications: Turbulent flow of water-based optimization (TFWO)," *Eng. Appl. Artif. Intell.*, vol. 92, p. 103666, 2020.

[25] M. E. Baran and F. F. Wu, "Network reconfiguration in distribution systems for loss reduction and load balancing," *IEEE Trans. Power Deliv.*, vol. 4, no. 2, pp. 1401–1407, 1989.

[26] M. E. Baran and F. F. Wu, "Optimal capacitor placement on radial distribution systems," *IEEE Trans. Power Deliv.*, vol. 4, no. 1, pp. 725–734, 1989.

[27] E. Ostadi, S. Jahanbakhsh, H. Rostamzadeh, M. Rezaibanafsheh, and A. M. Khorshiddust, "Spatio-temporal trend analysis of solid precipitation in northwest Iran," *Arab. J. Geosci.*, vol. 14, p. 1709, 2021.

[28] B. Salahi, "Detection of relationship between snowy days in ardabil province with bi-seasonal fluctuations of large-scale atmospheric-oceanic circulation patterns of Atlantic & Pacific oceans," *Geogr. Space*, vol. 22, pp. 139–159, 2022.